Poly(ε-caprolactone)-based nanofibrous scaffold incorporated with decellularized bone extracellular matrix as a potential strategy for bone regeneration

Ming Zhang
Department of Orthopaedics, Zhongda Hospital, School of Medicine, Southeast University
Quan Zhou
Department of Orthopaedic Surgery, The Affiliated Huai'an Hospital of Xuzhou Medical University, The Second People's Hospital of Huai'an
Qiangsheng Dong
School of Materials Science and Engineering, Jiangsu Key Laboratory for Advanced Metallic Materials, Southeast University. School of Materials Science and Engineering, Jiangsu Key Laboratory of Advanced Structural Materials and Application Technology, Nanjing Institute of Technology
Jue Zhang
Department of Orthopaedic Surgery, The Affiliated Jiangning Hospital of Nanjing Medical University
Xin Zhou
Department of Orthopaedic Surgery, The Affiliated Jiangning Hospital of Nanjing Medical University
Hao Huang
Department of Orthopaedic Surgery, The Affiliated Jiangning Hospital of Nanjing Medical University
Junchen Bao
Department of Orthopaedic Surgery, The Affiliated Jiangning Hospital of Nanjing Medical University
Hongjian Shan
Department of Orthopaedic Surgery, The Affiliated Jiangning Hospital of Nanjing Medical University
Furong Sun
Department of Orthopaedic Surgery, The Affiliated Jiangning Hospital of Nanjing Medical University
Liangliang Li (✉ lianglianglinj@163.com)
Department of Orthopaedic Surgery, The Affiliated Jiangning Hospital of Nanjing Medical University
https://orcid.org/0000-0001-7872-8681

Research Article

Keywords: Bone regeneration, Nanofibrous scaffold, decellularized extracellular matrix, poly(ε-caprolactone), Electrospinning

Posted Date: October 17th, 2022

DOI: https://doi.org/10.21203/rs.3.rs-2148105/v1

Abstract

Background: Critical size bone defect is still a great challenge in orthopedics. Scaffolds with nanofibrous microstructure seems a promising candidate for critical size bone defect repair. Here we fabricated poly(ε-caprolactone)-based nanofibrous scaffold incorporated with bone derived decellularized extracellular matrix (PCL/dB-ECM) to provide a suitable platform for bone regeneration.

Methods: dB-ECM was prepared first and different weight ratios of PCL and dB-ECM was blended to fabricate PCL/dB-ECM nanofibrous scaffolds by electrospinning. The physicochemical properties of the nanofibrous scaffolds were investigated. Rabbit bone mesenchymal stem cells (rBMSCs) were seeded on the nanofibrous scaffolds to evaluate cell proliferation, viability, morphology, cytoskeleton spread and osteogenic differentiation. The ability of the scaffolds to promote bone regeneration in vivo was also assessed by being implanted into a rabbit femoral condyle defect model.

Results: The microstructure of the PCL**/**dB-ECM (2:1) nanofibrous scaffold exhibited randomly arranged nanofibers interlaced to each other to form a network structure. The incorporation of dB-ECM into the scaffold improved the bioactivity of PCL, significantly enhanced the attachment, proliferation and cytoskeleton extension of rBMSCs, as well as remarkably promoted osteogenic differentiation of rBMSCs by elevating the expression of osteogenic-related genes and proteins and by enhancing the ALP activity and calcium deposition. Furthermore, in vivo assays demonstrated that PCL**/**dB-ECM (2:1) nanofibrous scaffold obviously facilitated new bone formation with better trabecular structures and excellent integration with the surrounding tissues.

Conclusion: The PCL**/**dB-ECM (2:1) nanofibrous scaffold showed excellent bioactivity to facilitate rBMSCs proliferation and osteogenic differentiation in vitro, as well as promoted new bone formation in vivo, suggesting the PCL-based nanofibrous scaffolds incorporated with dB-ECM could be a promising strategy for effective repair of bone defect.

1. Introduction

Critical size bone defect, which usually caused by traffic accident, bone tumor, and large-scale bone section, is still a great challenge in orthopedics[1, 2]. It was believed that there were more than two million patients were treated with bone grafts annually in the world and bone grafts market will reach 3.48 billion dollars by the end of 2023[3, 4]. Although autogenous bone graft is considered as the gold standard to repair the critical size bone defect, it has some disadvantages such as limited source of donor tissue, donor site morbidity and poor availability[4–6]. Therefore, it has become an urgent need to develop bioactive substitutes for bone defect repairment.

To address this problem, bone tissue engineering (BTE) has been developed aiming to create artificial substitutes for repairing critical size bone defect. Many novel methods or technologies have been introduced to fabricate scaffolds as alternatives to autogenous bone grafts, including three dimension

(3D) printing, electrospinning, freeze drying and selective laser sintering[7–9]. Electrospinning is an easy way to fabricate nanofibrous scaffold with high surface area-to-volume ratio and high inter-fiber distance, which can promote cell adhesion, proliferation and differentiation[10, 11]. More importantly, the electrospinning nanofibrous scaffold simulates the native structure of an extracellular matrix (ECM), which plays a key role in cell survival, migration and proliferation[11]. Hence, electrospinning has been widely used in the fields of drug delivery, wound dressing and engineering scaffold fabrication[12, 13].

The materials which were applied in BTE have been categorized into two kinds generally, natural polymers and synthesis polymers[14]. Due to their superior hydrophilicity, biocompatibility and osteoinductive, natural polymers such as collagen, gelatin, silk, hyaluronic acid, alginate and decellularized tissues are extensively used in the construction of BTE scaffolds. However, considering their antigenicity, poor mechanical properties and rapid degradation, natural polymers cannot fully meet the conditions of BTE scaffolds[15]. Synthesis polymers such as poly(ε-caprolactone) (PCL), poly(lactic acid) (PLA), poly(lactic-co-glycolic acid) (PLGA) and their copolymers, are promising materials for BTE scaffolds because of their excellent biocompatibility, controlled degradation and capability to serve as platform to achieve neovascularization and bone formation[16, 17]. Among these, PCL is well known as an aliphatic and semi-crystalline polymer, which exhibits good mechanical strength and superior biocompatibility and has been approved by the FDA for biomedical devices use[17, 18]. In addition to the above advantages, PCL can also provide a rough surface to facilitate initial cell anchoring[19]. Based on these advantages, PCL has been widely used to fabricate BTE scaffold in different forms. However, compared to natural polymers, pure PCL suffers from low hydrophilicity and insufficient biochemical activity, leading to limitation of scaffold-cell interaction and ECM deposition[20, 21]. So, PCL-based blend scaffold fabrication or surface modification strategies have been applied to improve the hydrophilicity and bioactivity of PCL[22, 23].

As mentioned above, decellularized extracellular matrix (dECM) is a kind of natural derived biomaterial and shows a promising application in the fields of regenerative medicine. By physical, chemical and enzymatic methods, the cells and their nuclear components were removed from tissues, while retaining tissue-specific ECM architecture and functional properties such as nanostructure, complex biochemical cues and bio inductive properties[24]. dECM has been isolated from a variety of different tissues or organs, including skin, adipose, meniscus, cartilage, bone and liver. It’s widely used in the fabrication of tissue regeneration engineering scaffold individually or incorporated with other materials[25–27]. Decellularized bone extracellular matrix (dB-ECM), which is derived from bone tissue, consisting of inorganic hydroxyapatite mineral and organic matrix components[28], has shown superior prospects in promoting stem cell adhesion, proliferation, and differentiation[6]. Owing to the incorporation of dB-ECM, we hypothesis that PCL and dB-ECM blending scaffold could not only overcome the poor hydrophilicity of PCL, but also introduce the bioactive factors into the scaffold, making it more suitable for cell adhesion and subsequent biological behavior, so as to promote bone regeneration.

In this work, as illustrated in Fig. 1, the dB-ECM was prepared successfully first, then the PCL/dB-ECM nanofibrous scaffolds with different ratio of PCL and dB-ECM were fabricated by electrospinning. In order to evaluate the effect of dB-ECM on the physicochemical properties and bioactivity of the nanofibrous scaffolds, the microstructure, hydrophilic, porosity and mechanical properties of the scaffolds were performed. In addition, the viability and osteogenic differentiation of rabbit bone mesenchymal stem cells (rBMSCs) seeding on the scaffolds were studied. Finally, the ability of the scaffolds to promote bone regeneration in vivo was also investigated by being implanted into a rabbit femoral condyle defect model. Based on this study, we hope it will provide a new insight into the construction of the BTE scaffolds.

2. Materials And Methods

2.1 Decellularization of cancellous bone

The decellularization process referred to several previous studies and made some changes[29–31]. Fresh cancellous bone samples were harvested from the femoral heads of five white swine weighing 50–60 kg from the local slaughterhouse within 24 h of slaughter. Thereafter, the cancellous bone samples were washed in phosphate-buffer saline (PBS; KeyGEN, Jiangsu, China) under continuous shaking for 4 h to remove excess blood, with changing PBS every hour. Then the combination of physical, chemical and enzymatic processing was operated to obtain the dB-ECM. Briefly, the cancellous bone samples were frozen at -80 ℃ until crystal formation followed by thawing at 37 ℃ for 2 h. This process was repeated two times. Then the samples were soaked in distilled water containing 0.1% sodium dodecyl sulfate (SDS; Sigma-Aldrich, MO, USA) at 37 ℃ for 24 h. Afterwards, the samples were washed for 30 minutes in PBS to completely remove SDS, with changing solution every 10 minutes. After being incubated in 1% Triton X-100 (Sigma-Aldrich, MO, USA) for 48 h, the samples were degreased with methyl alcohol for 24 h. Following a further 30 minutes washes in PBS the samples were processed with 100 U/ml DNase (Sigma-Aldrich, MO, USA) and 50 U/ml RNase (Sigma-Aldrich, MO, USA) at 37 ℃ for 4 h. Finally, after being washed with PBS under continuous shaking for 30 minutes twice, the dB-ECM were successfully prepared. The samples were dried and stored at 4 ℃ for further use.

2.2 Decellularization efficiency of dB-ECM

The absence of visible nuclei in tissue sections stained with hematoxylin and eosin (H&E) and 4',6-diamino-phenylindole (DAPI) was suggested as criteria of decellularization[30]. In addition, the residual DNA amount should be less than 50 ng per mg of dECM dry weight[32]. Therefore, in this part of the experiment, we performed histology and DNA content analysis of dB-ECM to evaluate the decellularization effect.

2.2.1 H&E and DAPI staining

The native bone tissue and dB-ECM were fixed in 4% paraformaldehyde for 48 h at room temperature and then decalcified with 10% EDTA (Sigma-Aldrich, MO, USA) at 4 ℃, with changing EDTA solution every two

days until the samples were soft enough to be sectioned with a scalpel. Then the samples were dehydrated stepwise using ethanol and embedded in paraffin and sectioned into 5 μm. After undergoing deparaffinized, rehydrated and washed in distilled water, the slides were stained with H&E to assess the cellular component and general structure of the dB-ECM. DAPI (KeyGEN, Jiangsu, China) staining was performed according to the manufacturer's instructions to identify the presence of any residual intact cell nuclei.

2.2.2 Quantification of residual DNA amount

To investigate the residual DNA amount of the native bone tissue (n = 6) and dB-ECM (n = 6), a DNA isolation reagent (Gibco BRL, MD, USA) was used to extract the genomic DNA according to the manufacturer's instructions. Briefly, the equal weight of dried samples was cut into thin strips and less than 25 mg in weight were homogenized in 1ml of DNAzol Reagent followed by DNA precipitation, DNA wash and solubilization. Then the extracted genomic DNA was quantitated by measuring absorbance at 260 nm in a multifunction microplate reader (BioTek, VT, USA). The DNA content was calculated according to the DNA concentration and the initial dry weight of the samples and expressed as ng/mg.

2.2.3 Collagen and calcium content analysis

In order to evaluate the retention of the bioactive components in dB-ECM, the content of collagen and calcium were also determined.

The Hydroxyproline assay kit (KeyGEN, Jiangsu, China) was used to quantify the collagen content of the native bone tissue and dB-ECM according to the manufacturer's instructions and others previous studies[33, 34]. The native bone tissue (n = 6) and dB-ECM (n = 6) were first weighed to achieve equal weight. Then the samples were acid hydrolyzed using 6 M hydrochloric acid (HCL) at 100 ℃ for 8 h followed by neutralized with sodium hydroxide (NaOH). The Edwards&O'Brien method was used to quantify the hydroxyproline content. In brief, standard concentrations were made from trans-4-hydroxy-L-proline firstly. Then 100 μl Oxidation solution (Chloramine-T in distilled water) was added to each standard and test samples (50 μl) in a flat bottom 96-well plate with agitation for 5 min. Ehrlich's reagent (100 μl) was then added and the plate was incubated at 60 ℃ for 45 min. Absorbance was read at 570 nm using a multifunction microplate reader (BioTek, VT, USA). The concentration of hydroxyproline in the samples was determined according to the established of the standard curve. A ratio of 7.2:1 for collagen-to-hydroxyproline was adopted to calculate the collagen content of the samples.

The native bone and dB-ECM samples were grinded into tiny particles with a mortar, respectively. An equal weight of lyophilized native bone and dB-ECM particles were solubilized in 0.5 M HCL at 4 ℃ until no visible particles remained. Calcium content in the solution was then quantified using inductively coupled plasma optical emission spectrometer (ICP-OES; Thermo Fisher Scientific, MA, USA).

2.3 Fabrication of nanofibrous scaffolds

Nanofibrous scaffolds were fabricated by electrospinning. Three groups were set in this study: PCL nanofibrous scaffold, PCL/dB-ECM (4:1) nanofibrous scaffold and PCL/dB-ECM (2:1) nanofibrous

scaffold. For PCL nanofibrous scaffold, 12% (w/v) PCL solution was prepared by dissolving PCL particles (molecular weight of 80000; Sigma-Aldrich, MO, USA) in 1,1,1,3,3,3-hexafluoro-2-propanol (HFP; Aladdin, Shanghai, China) for 12 h at room temperature with continuous agitation. Then the PCL solution was transferred to a 5 ml syringe with 16 gauge blunt-ended needle and positioned in a syringe pump at the flow rate of 1.0 ml/h for the electrospinning process. The aluminum foil was placed at a distance of 15 cm from the spinneret as a collector. A voltage of 20 KV was applied between the needle and ground collector. For PCL/dB-ECM (4:1) and PCL/dB-ECM (2:1) nanofibrous scaffolds, the dB-ECM particles were ground with a mortar and filtered through a 150-mesh screen to obtain the dB-ECM powders. Then the dB-ECM powders were added into 12% (w/v) PCL solution to obtain the blend solution with different weight ratio of PCL and dB-ECM (4:1 and 2:1), respectively. Following constant stirring, the uniform suspension without aggregation was obtained and injected into the syringe. Then the same procedure was operated to fabricate PCL/dB-ECM (4:1) and PCL/dB-ECM (2:1) nanofibrous scaffolds using electrospinning. The electrospinning process was carried out at room temperature and 40% humidity. The scaffolds were removed from the collector and dried in a vacuum oven overnight followed by storing in the desiccator for further use.

2.4 Characterization of nanofibrous scaffolds

2.4.1 Microstructure of nanofibrous scaffolds

The nanofibrous scaffolds were cut into 5 mm×5 mm discs and then gold-coated using a gold sputter coater. After that, the morphology of the nanofibrous scaffolds was observed using a scanning electron microscope (SEM; FEI Sirion, FEI, USA) at a voltage of 15 KV. The distribution of Ca and P elements in PCL/dB-ECM (4:1) and PCL/dB-ECM (2:1) nanofibrous scaffolds were detected by energy-dispersive spectrometer (EDS; Oxford Azter X-Max 80) coupled to SEM. The diameter distribution range and average diameter of nanofibers were calculated by randomly measuring 50 fibers from SEM micrographs using Image J software (National Institutes of Health, MD, USA).

2.4.2 Water contact angle measurement

The water contact angle (WAR) analysis system (SL200B; Solon Technology Science, Shanghai, China) was used to evaluate the hydrophilic property of the nanofibrous scaffolds. In brief, a 0.8 μl of distilled water was dropped onto the surface of scaffolds (15 mm×15 mm), and the angles between the water droplet and scaffold surface were measured. Six samples of each group were selected to test. The procedure was performed at room temperature and 50% humidity.

2.4.3 Porosity measurement

The AutoPore IV-9500 Mercury Porosimeters (Micromeritics, GA, USA) and mercury porosimetry analysis technique were used to evaluate the porosity of the nanofibrous scaffolds according to the manufacturer's instructions. All measurements were taken from six different samples each group.

2.4.4 Mechanical Characterization

The tensile strength of nanofibrous scaffolds was tested using a universal material tester (Jimtec, Beijing, China). In brief, samples of different groups were cut into rectangle shape with dimensions of 20 mm×30 mm followed by clamped to the device with two tensile grips. The tensile strength was performed under application of a 10 N tensile load and tensile speed of 1 mm/min. The stress-strain curves of the samples were recorded. According to the stress-strain curves, the ultimate tensile strength was obtained as the highest stress prior to the samples break. The elastic modulus was determined as the slope of the initial linear section of the curve, and the elongation (%) was calculated as the percentage elongation of the samples at the break.

2.5 In vitro cell study

2.5.1 Cell culture of rBMSCs

rBMSCs were isolated according to our previous publication[35]. The animal experiments involved in this study were approved by the Ethics Commission of Nanjing Medical University. rBMSCs were cultured in Dulbecco's modified eagle medium (DMEM; Gibco BRL, NY, USA) containing 10% fetal bovine serum, 100 U/ml penicillin and 100 mg/ml streptomycin at 37 ℃, 5% CO_2 and 95% humidity. Culture medium was changed every 3 days.

2.5.2 Cell seeding

The three groups of nanofibrous scaffolds were punched to obtain disks with 6 mm diameter and then placed in 96-well plates. The scaffolds were sterilized by exposing them to UV light for 1 h each side followed by immersing in 75% ethanol for 2 h and washed with PBS three times prior to cell seeding. The rBMSCs were seeded on the scaffolds at a density of 1×10^4 each well. 20 μl DMEM medium was added into each well and the cell-seeded scaffolds were incubated at 37 ℃, 5% CO_2 and 95% humidity for 2 h to allow cell initial attachment. After that, additional 100 μl fresh DMEM media was added into wells. The medium was changed every 3 days.

2.5.3 Cell proliferation

Cell proliferation of rBMSCs seeded on scaffolds at timepoints of 1, 3, 5, and 7 days was evaluated with cell counting kit-8 (CCK-8; Thermo Fisher Scientific, MA, USA) according to the manufacturer’s instructions. Briefly, the 20 μl CCK-8 agent was added into each well and co-cultured with rBMSCs seeded scaffolds at 37 ℃, 5% CO2 and 95% humidity for 4 h. After incubation, 200 μl solution of each well was transferred to a new 96-well plate, The absorbance was measured at 450 nm excitation wavelength using a multifunction microplate reader (BioTek, VT, USA). rBMSCs cultured in 96-well plate without nanofibrous scaffolds was established as a positive control group.

2..5.4 Cell viability

The cytotoxicity of the scaffolds was evaluated using Live-Dead kit (Thermo Fisher Scientific, MA, USA) at 3 and 7 days after rBMSCs seeded on scaffolds according to the manufacturer’s instructions. Briefly, at

the designed timepoints, the scaffolds were washed with PBS three times and incubated with staining solution of 4 mM calcein acetoxymethyl eater and 2 mM ethidium homodimer for 30 min at 37 ℃ away from light. After gently rinsed three times by PBS, the scaffolds were observed and images were captured using Confocal Laser Scanning Microscope (CLSM; Carl Zeiss, Baden-Württemberg, Germany). Quantitative analysis of cell viability was performed using Image J software (National Institutes of Health, MD, USA).

2.5.5 Cell morphology

After 3 and 7 days of seeding on scaffolds, the rBMSCs attachment status and morphology were assessed by SEM. The scaffolds were washed with PBS, fixed in 4% paraformaldehyde for 2 h and dehydrated in a series of graded concentrations of ethanol (70%, 80%, 90%, and 100%). After that, the samples were dried in air followed by gold sputter coating. The morphology of the samples was observed using SEM (FEI Sirion, FEI, USA).

2.5.6 F-actin observation

The rBMSCs attachment on scaffolds and cytoskeletal morphology were analyzed using F-actin staining. After co-cultured with rBMSCs for 3 and 7 days, the scaffolds were gently rinsed with PBS three times and fixed with 4% paraformaldehyde for 15 min. After being permeabilized with 0.1% Triton X-100 for 5 min, CoraLite®594 conjugated phalloidin (Proteintech, IL, USA) was used to stain the cytoskeletal protein for 20 min at room temperature. The nuclei were counterstained with DAPI (KeyGEN, Jiangsu, China) in the dark for 15 min at room temperature. The spread and extension of the cytoskeleton of rBMSCs were observed and images were captured using an inverted fluorescence microscope (Carl Zeiss, Baden-Württemberg, Germany).

2.6 Osteogenic differentiation of rBMSCs on nanofibrous scaffolds

In order to evaluate the effect of scaffolds on osteogenic differentiation of rBMSCs in vitro, we carried out the following studies.

2.6.1 Alkaline phosphatase (ALP) activity analysis

At 7 days after rBMSCs seeded on scaffolds and cultured in osteogenic induction medium, azo coupling method was performed to evaluate the ALP activity using Alkaline phosphatase staining solution (Solarbio, Beijing, China) according to the manufacturer's instructions. In brief, the co-cultured scaffolds were rinsed by PBS gently and fixed with ALP stationary solution for 3 min. After washing by PBS for 15 seconds, the co-cultured scaffolds were incubated in ALP incubation solution for 15 min followed by washing with PBS. The ALP positive staining was observed using an optical microscope and the images were captured. The semiquantitative analysis of ALP activity was also measured by p-nitrophenyl phosphate using Bicinchoninic Acid assay kit (Beyotime, Shanghai, China) according to our previous

publication[35]. The ALP activity was normalized to the total protein content and expressed as μmol/hr/mg protein.

2.6.2 Alizarin Red S (ARS) staining

ARS staining was performed to assess the calcium deposition of the rBMSCs seeded on scaffolds using Alizarin Red S Staining Kit (Beyotime, Shanghai, China) according to the manufacturer's instructions. Briefly, 21 days after culturing, the scaffolds were rinsed by PBS and fixed with 4% paraformaldehyde for 20 min. Then 2% ARS staining solution was added into the well to fully cover the scaffolds for 30 min at room temperature. Positive staining was observed using an optical microscope and the images were captured. The semiquantitative analysis of ARS was performed as previously reported[36]. In brief, 10% cetylpyridinium chloride (Sigma-Aldrich, MO, USA) was used to desorbed the staining and the solution was analyzed for absorbance reading at 590 nm using a multifunction microplate reader (BioTek, VT, USA). The levels of ARS were normalized to the total protein content.

2.6.3 Quantitative real-time reverse transcription polymerase chain reaction (qRT-PCR) analysis of osteogenic-related gene expression

Osteogenic-related gene expression analysis was performed after rBMSCs were cultured on the scaffolds for 14 days. Total RNA was extracted from co-cultured scaffolds using TRIzol Reagent (Thermo Fisher Scientific, MA, USA). The concentration of RNA was measured at 260nm optical density. RNA was processed to reverse transcribe to cDNA using SuperScript (Thermo Fisher Scientific, MA, USA). Quantitative PCR was performed with SYBR green reaction mix (Thermo Fisher Scientific, MA, USA) using a Step One Real-Time PCR System (Thermo Fisher Scientific, MA, USA). Triplicates were performed for each sample, and the expressions of target genes were normalized to the corresponding GAPDH and analyzed using the $2^{-\triangle\triangle CT}$ formula. The primer sequences were listed in Table 1.

Table 1
Primer sequences used for qRT-PCR

Genes	Forward (5'-3')	Reverse (5'-3')
Col1	CTTCTGGCCCTGCTGAAAGGATG	CCCGGATACAGGTTTCGCCAGTAG
Runx2	TCAGGCATGTCCCTCGGTAT	TGGCAGGTAGGTATGGTAGTGG
Ocn	CCGGGAGCAGTGTGAGCTTA	TCAGGCATGTCCCTCGGTAT

Table 1. Primer sequences used for qRT-PCR

2.6.4 Immunofluorescence staining of osteogenic-related proteins

Osteogenic-related proteins, such as Col1 and Runx2 were further detected by immunofluorescence staining to deeper evaluate the osteogenic differentiation of rBMSCs cultured on nanofibrous scaffolds. After 14 days co-cultured with rBMSCs, the scaffolds were fixed in 4% paraformaldehyde for 1 h and rinsed gently with PBS three times. After treatment with 0.1% Triton-X100 (Beyotime, Shanghai, China) for 15 min, the scaffolds were immersed in 3% bovine serum albumin (BSA; Beyotime, Shanghai, China) solution for 1 h at room temperature. Then the scaffolds were incubated with primary antibodies (Col1, 1:1000; Runx2, 1:500; All purchased from Proteintech, IL, USA) at 4 ℃ overnight followed with incubation of secondary antibodies (CoraLite488-conjugated affinipure goat anti-mouse IgG, 1:500; CoraLite488-conjugated affinipure goat anti-rabbit IgG, 1:500; All purchased from Proteintech, IL, USA) for 1 h at room temperature. To stain the nuclei, DAPI (KeyGEN, Jiangsu, China) was added onto the scaffolds and incubated for 20 min at room temperature avoiding the light. The scaffolds were then washed three times and the images were captured using an inverted fluorescence microscope (Carl Zeiss, Baden-Württemberg, Germany). The semiquantitative analysis of the protein expression of Col1 and Runx2 in rBMSCs cultured on nanofibrous scaffolds was determined using Image J software (National Institutes of Health, MD, USA) by calculating mean fluorescence intensity of the images.

2.7 In vivo animal model experiments

A total of 20 female New Zealand white rabbits at the age of six months were used to establish the bone defect model. All animal experiments were approved by the Institutional Animal Experiment Committee of Nanjing Medical University.

The rabbits were randomly divided into scaffold implanted groups (PCL, n = 5; PCL/dB-ECM (4:1), n = 5; PCL/dB-ECM (2:1), n = 5) as well as blank control group (bone defect alone without implants, n = 5). After generally anesthetized by injecting 10% chloral hydrate (4 ml/kg body weight), the knees of the rabbits were shaved and disinfected with iodophor, and a medial para-patellar skin incision was made to expose femoral condyle. Then, a cylindrical bone defect with 4 mm in diameter and 4 mm in depth was created by a slow speed electric drill. To ensure the defect zone was completely filled, the scaffolds were rolled into a cylinder with the same size as the bone defect and then implanted into the defect site, while no scaffold was implanted into blank control group. After washing with sterile normal saline, the knee joint capsule, subcutaneous fascia and skin were sutured layer by layer with 4 − 0 absorbable suture.

The rabbits were euthanized at 12 weeks post-surgery and the femoral condyle was harvested for further analysis.

2.8 Micro-computed tomography (Micro-CT) assessment

Micro-CT was used to assess the formation and density of mineralized tissue in defect site. The femoral condyle was fixed in 4% paraformaldehyde for 24 h and then evaluated by Micro-CT scanner (Siemens, Germany) at a resolution of 15 μm and a voltage of 80 kV. The region of interest (ROI) was defined as a cylindrical with a diameter of 4 mm and depth of 4 mm at the bone defect site. The images were analyzed by Micro-CT image analysis software (Siemens Inveon Research Workplace) and data including

mineralized callus volume fraction (BV/TV, %), Trabecular Number (Tb. N, 1/mm), Trabecular separation (Tb. Sp, mm) and Bone Mineral Density (BMD, g/cm^3) were obtained.

2.9 Histological analysis

After Micro-CT scan was accomplished, the samples were dehydrated with graded ethanol series, decalcified in 10% ethylenediaminetetraacetic acid (EDTA) solution until the blade can easily cut the samples, and embedded in paraffin. The samples were then cut into 5 μm sections for H&E and Masson trichrome staining to evaluate the morphology structure and collagen fibers distribution of the regenerated tissues at the defect site. After staining, the sections were mounted with gum and observed by optical microscopy.

2.10 Statistical analysis

All data were presented as means ± standard deviation. Student's t-test was conducted to evaluate the statistical significance between two groups and one-way ANOVA was performed for three or more groups. $p < 0.05$ was considered as a significant difference.

3. Results

3.1 Characterization of dB-ECM

Through the combination of physical, chemical and enzymatic methods, the decellularized bone extracellular matrix was prepared successfully. Gross examination indicated that the dB-ECM specimens were yellowish white in color (Fig. 2A). By grinding in a mortar and filtering through a 150-mesh screen, the dB-ECM powders were obtained (Fig. 2B).

The H&E staining, DAPI and DNA quantitation were performed to evaluate the decellularization effect of dB-ECM. H&E staining showed the nuclei in dB-ECM were almost completely removed from the cells (Fig. 2C). On the other hand, the natural architecture and bone matrix were well reserved in dB-ECM (Fig. 2C). The DAPI staining further confirmed that the native bone tissue contains amounts of cell nuclei, on the contrary, there were no cell nuclei debris observed in dB-ECM (Fig. 2C). Besides, the DNA quantification assay revealed that the amount of DNA in native bone tissue was 253.67 ± 15.58 ng/mg (Fig. 2D), while the residual DNA amount in dB-ECM was 23.17 ± 5.83 ng/mg (Fig. 2D), which met the standard that the residual DNA amount should be less than 50 ng per mg of dB-ECM dry weight, suggesting the complete removal of cell debris.

In order to assess the ECM major components preservation, the collagen content and calcium content in the native bone tissue and dB-ECM were detected. The results showed that the content of collagen was 95.83 ± 4.97 μg/mg and 84.17 ± 5.74 μg/mg in native bone tissue and dB-ECM, respectively, and there was no significant difference between the two groups ($p > 0.05$) (Fig. 2E). The analysis of calcium content exhibited that no significant difference was found between native bone tissue and dB-ECM (139.67 ± 6.98 μg/mg and 132.50 ± 8.27 μg/mg, respectively; $p > 0.05$) (Fig. 2F).

The above results confirmed that the dB-ECM exhibited good decellularization effect and relatively retained the bone matrix structure and components of native bone tissue.

3.2 Characterization of the electrospinning nanofibrous scaffolds

3.2.1 Microstructure of the nanofibrous scaffolds

The PCL and PCL/dB-ECM nanofibrous scaffolds were fabricated successfully by electrospinning. Figure 3A showed the microstructure of the three groups of nanofibrous scaffolds and distribution of dB-ECM particles in PCL/dB-ECM (4:1) and PCL/dB-ECM (2:1) nanofibrous scaffolds. All of the nanofibrous scaffolds consisted of randomly distributed nanofibers with uniform thickness, which intertwined with each other to form a network. The PCL/dB-ECM (4:1) and PCL/dB-ECM (2:1) nanofibrous scaffolds exhibited relatively uniform distribution of dB-ECM particles except for a little agglomeration. Moreover, the number of dB-ECM particles in PCL/dB-ECM (2:1) nanofibrous scaffold was much larger than that of PCL/dB-ECM (4:1) nanofibrous scaffold, which was further confirmed by EDS mapping of Ca and P elements, as shown in Fig. 3B, where Ca and P elements distributed uniform in nanofibers. By Image J software analysis, the nanofibers diameter of the PCL/dB-ECM (2:1) nanofibrous scaffold was mostly distributed in the range of 500 nm to 650 nm, which was closed to that of PCL and PCL/dB-ECM (4:1) nanofibrous scaffolds (500 nm to 700 nm and 400 nm to 700 nm, respectively) (Fig. 3C). However, as exhibited in Fig. 3D, with the increase of the dB-ECM content, the average diameter of the nanofibers became smaller. The average diameters of the nanofibers for PCL, PCL/dB-ECM (4:1) and PCL/dB-ECM (2:1) nanofibrous scaffolds were 639.16 ± 124.05 nm, 604.60 ± 121.54 nm and 580.90 ± 83.12 nm, respectively, and there was a significant difference between the PCL/dB-ECM (2:1) and PCL nanofibrous scaffolds ($p < 0.01$).

3.2.2 Hydrophilicity, porosity and mechanical test of the nanofibrous scaffolds

About the hydrophilicity analysis, as shown in Fig. 4A and B, the PCL nanofibrous scaffold was highly hydrophobic. The water contact angle of PCL nanofibrous scaffold was 127.61°±7.48°. With the increase of dB-ECM content, the PCL/dB-ECM (4:1) and PCL/dB-ECM (2:1) nanofibrous scaffolds tend to be more hydrophilic and the water contact angles were 83.10°±4.55° and 50.94°±12.23°, respectively (Fig. 4A). A significant difference was found between the PCL/dB-ECM (2:1) nanofibrous scaffold and the other two scaffolds ($p < 0.01$) (Fig. 4B), indicating that PCL/dB-ECM (2:1) nanofibrous scaffold had optimal hydrophilic properties.

The porosity results which were illustrated in Fig. 4C showed that the porosity was 79.99%±5.37%, 85.93%±2.95% and 91.42%±2.04% for PCL, PCL/dB-ECM (4:1) and PCL/dB-ECM (2:1) nanofibrous scaffolds, respectively, exhibiting a trend of increased porosity with the increase of dB-ECM content. In comparison with PCL and PCL/dB-ECM (4:1) nanofibrous scaffolds, the PCL/dB-ECM (2:1) nanofibrous

scaffold had much higher porosity, which means higher surface area-to-volume ratio and promotion of cell adhesion.

The mechanical test results were illustrated in Fig. 4D-G. As the stress-strain curve indicated (Fig. 4D), the mean elastic modulus of PCL, PCL/dB-ECM (4:1) and PCL/dB-ECM (2:1) nanofibrous scaffolds were 2.53 ± 0.17, 5.54 ± 0.14 and 2.15 ± 0.12 MPa, respectively, while the tensile strength of PCL, PCL/dB-ECM (4:1) and PCL/dB-ECM (2:1) nanofibrous scaffolds were 3.45 ± 0.12, 2.89 ± 0.08 and 2.20 ± 0.08 MPa, respectively (Fig. 4E and F). The PCL/dB-ECM (2:1) nanofibrous scaffold had the lowest elastic modulus and tensile strength compared with that of the other scaffolds. In contrast, the elongation rate of PCL/dB-ECM (2:1) nanofibrous scaffold (48.90%±1.10%) was significantly higher than that of PCL (28.02% ±0.61%) and PCL/dB-ECM (4:1) nanofibrous scaffolds (41.23%±0.91%) (Fig. 4G).

3.3 Biological assessment of nanofibrous scaffolds in vitro

3.3.1 Cell proliferation

The proliferation of rBMSCs cultured on scaffolds was tested at 1, 3, 5 and 7 days after seeding by CCK-8 assay. As shown in Fig. 5, rBMSCs cultured on all of the scaffolds exhibited increased proliferation rates at both timepoints, indicating that the scaffolds had good cytocompatibility. However, PCL nanofibrous scaffold showed the lowest cell proliferation rates throughout the experiment, which further proved that the poor hydrophilicity of PCL had a negative effect on cell adhesion and proliferation. Compared with the other two scaffolds, rBMSCs cultured on PCL/dB-ECM (2:1) nanofibrous scaffold had the highest cell proliferation rates at both timepoints, suggesting that PCL/dB-ECM (2:1) nanofibrous scaffold was the most suitable of the tested scaffolds for rBMSCs proliferation, probably due to the improvement of hydrophilicity of the nanofibrous scaffold by incorporating of appropriate amount of dB-ECM, which had been confirmed by previous hydrophilic test of the scaffolds.

3.3.2 Cell viability

Live-Dead assay was used to evaluate the cell viability after the rBMSCs and nanofibrous scaffolds were co-cultured for 3 and 7 days. As shown in Fig. 6A, after co-cultured for 3 days, there was only a small number of dead cells stained with red fluorescence were found in all of the nanofibrous scaffolds. On the contrary, a large amount of green fluorescence staining, which indicating live cells, could be seen in the three groups of nanofibrous scaffolds. On day 7, the number of live cells in all of the scaffolds increased significantly, further confirming that the nanofibrous scaffolds had excellent biocompatibility (Fig. 6B). Notably, rBMSCs cultured on PCL/dB-ECM (2:1) and PCL/dB-ECM (4:1) nanofibrous scaffolds exhibited significantly higher number of live cells compared with PCL nanofibrous scaffold. In particular, the largest number of live cells could be found spreading on the surface of PCL/dB-ECM (2:1) nanofibrous scaffold at both timepoints compared with PCL and PCL/dB-ECM (4:1) nanofibrous scaffolds, while the least number of dead cells, suggesting that PCL/dB-ECM (2:1) nanofibrous scaffold provided a more suitable microenvironment for promoting rBMSCs proliferation. Figure 6C and D illustrated the quantification of rBMSCs viability calculated from Live-Dead images with Image J after 3 and 7 days cultured on

nanofibrous scaffolds, respectively. The rBMSCs viability reached over 80% after 3 days cultured on PCL/dB-ECM (2:1) nanofibrous scaffold, which was significantly higher than that of PCL and PCL/dB-ECM (4:1) nanofibrous scaffolds. On day 7, the viability of rBMSCs cultured on PCL/dB-ECM (2:1) nanofibrous scaffold (93.09 ± 0.25%) also showed significantly higher than that of PCL (71.30 ± 3.40%) and PCL/dB-ECM (4:1) nanofibrous scaffolds (83.35 ± 0.53%), indicating that incorporation of appropriate content of dB-ECM enhanced cytocompatibility of the nanofibrous scaffolds.

3.3.3 Cell morphology observation

The morphology of rBMSCs cultured on nanofibrous scaffolds for 3 and 7 days, which was illustrated in Fig. 7A, showed the cells spread flat on all of the nanofibrous scaffolds. It was noticeable that more cells could be observed on the surface of PCL/dB-ECM (2:1) nanofibrous scaffold at both timepoints compared with that of the other two groups of scaffolds. Especially after 7 days culturing, the cells on PCL/dB-ECM (2:1) nanofibrous scaffold stretched and extended to a wider range, almost covering the whole surface of the scaffold. This finding was consistent with our CCK-8 (Fig. 5) and Live-Dead results (Fig. 6), further confirming that PCL/dB-ECM (2:1) nanofibrous scaffold had excellent cytocompatibility, as well as promoting cells attachment and spread.

The cytoskeleton spread and extension of rBMSCs cultured on nanofibrous scaffolds on day 3 and day 7 were evaluated by F-actin staining, which was illustrated in Fig. 7B. It was obviously that a remarkable increase of cells can be found attached to the PCL/dB-ECM (2:1) nanofibrous scaffold compared with that of PCL and PCL/dB-ECM (4:1) nanofibrous scaffolds at both timepoints, which was in accord with the results of Live-Dead (Fig. 6) and SEM (Fig. 7A). Moreover, on day 7, the actin cytoskeleton of rBMSCs cultured on PCL/dB-ECM (2:1) nanofibrous scaffold showed a wider stretch range and a more parallel arrangement in comparison with PCL and PCL/dB-ECM (4:1) nanofibrous scaffolds. The quantitative analysis of actin area was illustrated in Fig. 7C and D. On day 3, the actin area of rBMSCs cultured on PCL/dB-ECM (2:1) nanofibrous scaffold reached nearly 30%, which was significantly higher than that of PCL and PCL/dB-ECM (4:1) nanofibrous scaffolds (Fig. 7C). On day 7, the actin area of rBMSCs cultured on PCL/dB-ECM (2:1) nanofibrous scaffold (59.23 ± 1.51%) was also remarkably higher than that of PCL (21.24 ± 3.30%) and PCL/dB-ECM (4:1) nanofibrous scaffolds (39.18 ± 2.13%) (Fig. 7D). The results further indicated that incorporation of appropriate content of dB-ECM enhanced adhesion, proliferation and the cytoskeleton extension of rBMSCs on the surface of scaffolds.

Taken together, the data from the present study indicated that PCL/dB-ECM (2:1) nanofibrous scaffold had excellent cytocompatibility for the growth of rBMSCs. And compared with the other two groups of scaffolds, at the early stage of rBMSCs seeding, the incorporation of appropriate ratio of dB-ECM enhanced cell adhesion, spreading and cytoskeleton extension on the surface of PCL/dB-ECM (2:1) nanofibrous scaffold, therefore significantly promoted cell proliferation in the subsequent culture process.

3.3.4 Osteogenic differentiation of rBMSCs on nanofibrous scaffolds

ALP activity was performed to evaluate the osteogenic differentiation of rBMSCs seeded on nanofibrous scaffolds. As shown in Fig. 8A, the ALP staining exhibited more significant enhancement in PCL/dB-ECM (2:1) nanofibrous scaffold compared with that of PCL and PCL/dB-ECM (4:1) nanofibrous scaffolds. The result of semiquantitative analysis of ALP activity was illustrated in Fig. 8B, showed a significant higher ALP activity in PCL/dB-ECM (2:1) nanofibrous scaffold than that of the other two scaffolds.

As well as ALP activity assay, ARS staining was also used as marker of osteogenic differentiation. As shown in Fig. 8A and C, the ARS staining and semiquantitative analysis exhibited remarkably higher calcium deposition in PCL/dB-ECM (2:1) nanofibrous scaffold than that of PCL and PCL/dB-ECM (4:1) nanofibrous scaffolds.

To further evaluate the osteogenic differentiation of rBMSCs cultured on different groups of nanofibrous scaffolds, the expression of osteogenic specific genes of rBMSCs were detected by qRT-PCR after 14 days incubation in osteogenic medium. As illustrated in Fig. 8D-F, rBMSCs cultured on PCL nanofibrous scaffold had the lowest expression levels of Col1, Runx2 and Ocn, while the gene expression of Col1, Runx2 and Ocn were significantly upregulated in rBMSCs cultured on PCL/dB-ECM (4:1) and PCL/dB-ECM (2:1) nanofibrous scaffolds. Notably, rBMSCs cultured on PCL/dB-ECM (2:1) nanofibrous scaffold exhibited the highest expression levels of osteogenic specific genes, suggesting PCL/dB-ECM (2:1) nanofibrous scaffold enhanced osteogenic differentiation of rBMSCs greatly.

Moreover, the above results were further confirmed by immunofluorescence staining of osteogenic related proteins, which was illustrated in Fig. 8G. The PCL/dB-ECM (2:1) nanofibrous scaffold was observed to significantly enhance the protein expression of Col1 and Runx2 in rBMSCs in comparison with that of PCL and PCL/dB-ECM (4:1) nanofibrous scaffolds (Fig. 8G). As shown in Fig. 8H and I, the semiquantitative analysis, which was expressed as mean fluorescence intensity, displayed notably increased of Col1 and Runx2 expression in rBMSCs cultured on PCL/dB-ECM (2:1) nanofibrous scaffold, further indicating that PCL/dB-ECM (2:1) nanofibrous scaffold could significantly promote rBMSCs osteogenic differentiation.

In summary, due to the incorporation of dB-ECM, rBMSCs cultured on PCL/dB-ECM (2:1) and PCL/dB-ECM (4:1) nanofibrous scaffolds showed much better osteogenic differentiation than that of PCL nanofibrous scaffold, no matter at the level of osteogenic related genes or proteins. Additionally, the data indicated that PCL/dB-ECM (2:1) nanofibrous scaffold performed the best in promoting osteogenic differentiation of rBMSCs.

3.4 In vivo implantation

To evaluate the osteogenesis effect of the nanofibrous scaffolds in vivo, a bone defect model was created in the femoral condyle of rabbit. Then the nanofibrous scaffolds were implanted in the defect zone and gross observation, Micro-CT evaluation and histology assessment were performed at 12 weeks post-implantation.

The gross observation, which was illustrated in Fig. 9A, exhibited obviously that the PCL/dB-ECM (2:1) nanofibrous scaffold promoted better osteogenesis in comparison with the control group and other scaffolds implanted groups. In the control group, the defect zone was covered with new formation tissue with uneven surface, and a circle boundary can be seen clearly between the new tissue and the native bone tissue. It seemed that the PCL nanofibrous scaffold may hardly be degraded, and there was still part of PCL nanofibrous scaffold remaining in the defect area. Even if the defect area was not completely filled with new tissue, the healing of the bone defect in the PCL/dB-ECM (4:1) nanofibrous scaffold group was still significantly better than that of the control group and PCL nanofibrous scaffold group. The bone defect which was treated with PCL/dB-ECM (2:1) nanofibrous scaffold showed a normal bone morphology, which exhibited a healthy-looking and smooth surface, and the boundary surrounding the defect zone disappeared, indicating an excellent integration between the new tissue and the native bone tissue.

Micro-CT analysis was performed to observe the new bone formation within the defect site. As illustrated in Fig. 9B, the control group and PCL nanofibrous scaffold group demonstrated extremely insufficient bone regeneration. In contrast, PCL/dB-ECM (4:1) and PCL/dB-ECM (2:1) nanofibrous scaffolds groups showed much more regenerated bone (Fig. 9B). Notably, PCL/dB-ECM (2:1) nanofibrous scaffold group exhibited extensive bone regeneration in the defect site in comparison with PCL/dB-ECM (4:1) nanofibrous scaffold group (Fig. 9B). More importantly, the microstructure of the regenerated trabecular in PCL/dB-ECM (2:1) nanofibrous scaffold group, such as arrangement, interconnection and shape, was more similar to the surrounding native trabecular tissues, further indicating the great osteointegration of the PCL/dB-ECM (2:1) nanofibrous scaffold (Fig. 9B). The quantitative analysis of new bone formation showed significantly higher bone volume ratio, trabecular number, bone mineral density, and lower trabecular separation in the PCL/dB-ECM (2:1) nanofibrous scaffold group compared with the control group and PCL nanofibrous scaffold group (Fig. 9C). Although the new bone formation was notably increased in the PCL/dB-ECM (4:1) nanofibrous scaffold group compared with the control group and PCL nanofibrous scaffold group, the bone volume ratio, trabecular number and bone mineral density were still much lower than the PCL/dB-ECM (2:1) nanofibrous scaffold group (Fig. 9C).

The Micro-CT results were further supported by the histology evaluation of new bone formation, which was illustrated in Fig. 9D and E. As shown in Fig. 9D, H&E staining images showed that the defect site was filled with amorphous and irregular fibrous tissue in control group and PCL nanofibrous scaffold group, while PCL/dB-ECM (4:1) and PCL/dB-ECM (2:1) nanofibrous scaffolds groups showed much better trabecular structures, which was consistent with the results of Micro-CT (Fig. 9B). As shown in Masson trichrome staining images in Fig. 9E, the PCL nanofibrous scaffold group exhibited a few bone collagen fibers stained in green at the bottom of the defect site, which slightly better than the control group. However, in comparison with PCL/dB-ECM (4:1) and PCL/dB-ECM (2:1) nanofibrous scaffolds group, PCL nanofibrous scaffold group demonstrated extremely insufficient bone regeneration efficiency. The incorporation of dB-ECM to the scaffold lead to the superior regenerated bone with a smooth surface, good trabecular structures and excellent integration with the surrounding tissues (Fig. 9E). Furthermore,

due to the increase of dB-ECM content, PCL/dB-ECM (2:1) nanofibrous scaffold group exhibited much more regenerated bone than that of PCL/dB-ECM (4:1) nanofibrous scaffold group (Fig. 9E).

4. Discussion

It has been estimated that there will be about 28 million orthopedic surgery procedures worldwide by 2022, and a critical issue is the demand for bone substitutes will greatly increase, which is the second most transplanted tissue annually now[37]. Due to the drawbacks of immune response, donor site morbidity and shortage of supply, it seems that autografts and allograft will not fully cover the needs of bone transplantation[38, 39]. Therefore, BTE, which aims to fabricate bioactive bone scaffold for substitutions of bone tissue, is showing a promising prospect in repairing bone defect.

It is well-accepted that scaffolds, cells and growth factors are three elements for bone tissue engineering strategies. Among them, scaffolds play a key role in the realization of bone regeneration as they provide a suitable microenvironment for cells adhesion, proliferation, migration and differentiation[40]. The external shape, internal pores, mechanical properties and biocompatibility of the scaffolds directly affect the fate of cells, subsequently decide the effect of bone regeneration[41, 42]. Scaffolds with nano-scale topography are considered as a promising substrate for bone regeneration as they imitate the structure of natural bone extracellular matrix and interlaced collagen fibers, making them more beneficial to cell recruitment and adhesion[43, 44]. Electrospinning can fabricate nano-scale fibrous scaffolds with large surface area, high distance between fibers for cell gas exchange, infiltration and nutrition[38]. On the other hand, the equipment for electrospinning is cheap and easily available. Due to the above advantages, electrospinning has attracted great attention in BTE scaffold construction. Previous studies have illustrated that electrospinning nanofibers could create suitable surface for cell attachment and enhance osteogenic differentiation of MSCs in vitro[45, 46]. In the present study, we fabricated nanofibrous scaffolds using electrospinning and our results showed that the scaffolds exhibited randomly arranged nanofibers interlaced to each other to form a network structure, which may effectively promote cell diffusion and contribute to the cell adhesion, extracellular matrix secretion and protein adsorption because of a larger specific surface area[47].

Even though a wide range of biomaterials, including natural polymers, synthetic polymers, inorganic biomaterials and some of their blends, have been investigated for BTE scaffold construction, researchers have not reached a consensus on the choice of biomaterials due to the advantages and disadvantages of each material[48, 49]. As a kind of synthetic polymer, PCL has been approved by FDA in the field of BTE because of its good biocompatibility, biodegradability and excellent mechanical properties. Compared to bioceramics, PCL can be degraded gradually in the body. More importantly, the degradation products are non-toxic. In addition, PCL has better mechanical properties and exhibits easier handing process in comparison with other synthetic polymers. However, the hydrophobic nature of PCL inhibits cell attachment and therefore proliferation[14], which can be solved by combining with other biomaterials, such as bioceramics, natural polymers and inorganic compounds[47, 50]. Therefore, in the present study,

different concentration of dB-ECM was introduced to obtain PCL/dB-ECM blend to improve the hydrophilic properties and bioactivity of pure PCL. Our data showed that the PCL nanofibrous scaffold was hydrophobic, whereas the incorporation of dB-ECM greatly decreased water contact angle of the PCL/dB-ECM nanofibrous scaffolds. Notably, the water contact angle decreased gradually with the increase of dB-ECM content and the PCL/dB-ECM (2:1) nanofibrous scaffold exhibited the optimal hydrophilicity in comparison with PCL/dB-ECM (4:1) nanofibrous scaffold, indicating that appropriate dB-ECM content played an important role in enhancing hydrophilic of the PCL/dB-ECM nanofibrous scaffolds. Meanwhile, the incorporation of dB-ECM resulted in a higher porosity of PCL/dB-ECM (2:1) nanofibrous scaffold, which was inclined to enhance cell proliferation and migration. However, as previously study demonstrated, excessive porosity also brings some disadvantages, such as affecting the mechanical properties of the scaffold[47]. The mechanical test results of the present study showed that the PCL/dB-ECM (2:1) nanofibrous scaffold had the lowest elastic modulus and tensile strength, which may due to the incorporation of dB-ECM particles impaired the integrity of the scaffold microstructure, thus reducing the mechanical performance. Some previous materials have shown good osteogenic differentiation potential in vitro, but failed when implanted in vivo because of the imbalance between microstructure and mechanical properties[51]. Therefore, in the process of BTE scaffolds fabrication, the mechanical properties need to be taken into consideration when designing scaffold architecture[51].

Biocompatibility is the key index to evaluate the performance of the BTE scaffolds. Bio-incompatibility may lead to inflammation, immune response and tumor formation. It was believed that the inflammation reaction caused by scaffold should be resolved within 14 days, and chronic inflammation could result in an infection[51]. It has been proven that PCL exhibited good biocompatibility and widely used as a safe biomaterial in BTE filed[52, 53]. In this study, in order to ensure the biocompatibility of the PCL/dB-ECM nanofibrous scaffolds, we must first prepare dB-ECM effectively and safely. So, the chemical, physical and enzymatic methods were combined to completely remove cells from bone tissue, so as to avoid its immunogenicity. The characterization analysis of dB-ECM proved that it not only achieved a satisfactory decellularize effect, but also retained the microstructure and major components of natural bone ECM, which laid a foundation for subsequent biological experiments. The CCK-8 results showed that rBMSCs cultured on PCL/dB-ECM (2:1) nanofibrous scaffold exhibited the highest cell viability and proliferation rates at 5 and 7 days of co-culturing, suggesting that PCL/dB-ECM (2:1) nanofibrous scaffold had an excellent biocompatibility, which was further confirmed by the Live-Dead test. After 7 days co-cultured with rBMSCs, the number of live cells in the PCL/dB-ECM (2:1) nanofibrous scaffold increased significantly compared with 3 days of culturing, and the PCL/dB-ECM (2:1) nanofibrous scaffold exhibited the highest number of live cells in comparison with the other scaffolds, while only a few dead cells. Taken together, the incorporation of dB-ECM into the nanofibrous scaffolds did not show any cytotoxicity, which indicated the effectiveness of the decellularize process and the safety of dB-ECM. On the other hand, the results of biological assessment further confirmed that the incorporation of dB-ECM enhanced the rBMSCs adhesion and proliferation in nanofibrous scaffolds.

It has been realized that each tissue has its specific ECM structure and composition that modulates cells response and benefits cells survival within that tissue[29, 54]. ECM exhibits tissue regeneration capabilities by directing seed stem cells to differentiate into tissue specific cell lines even without exogenous growth factors[29]. dB-ECM is a bone-derived biomaterial that can be used alone or in combination with other materials for BTE. Compared with other biomaterials, the main advantage of dB-ECM is that it retains the natural microenvironment, biochemical signals and physiological cues of bone tissue, which can promote cell growth and viability, thereby promoting bone regeneration[31, 55, 56]. The incorporation of dB-ECM into other biomaterials to fabricate scaffolds could mimic the native bone tissue microenvironment and introduce additional functional groups, which may facilitate initial adhesion and anchor of cells, showing a promising way to construct BTE scaffolds. Numerous studies which focused on dB-ECM have demonstrated that the scaffolds incorporated with dB-ECM can significantly enhance the expression of osteogenic gene marker when co-cultured with MSCs, as well as promoting bone regeneration in vivo[7, 57]. Consistent with the previous findings, our study confirmed that the incorporation of dB-ECM not only improved the bioactivity of PCL, but also enhanced the osteogenic differentiation of rBMSCs in vitro. The rBMSCs cultured on the PCL/dB-ECM (2:1) nanofibrous scaffold exhibited higher ALP activity and more calcium deposition, as well as upregulated expression of osteogenic related genes and proteins. In the present cytoskeletal morphology study, it's notable that the actin cytoskeleton of rBMSCs cultured on PCL/dB-ECM (2:1) nanofibrous scaffold showed a more orderly and parallel arrangement in comparison with the other scaffolds. This reminded us that the incorporation of dB-ECM may made positive contributions to affect the arrangement of intracellular cytoskeleton, which may be one of the reasons why dB-ECM can enhance cell adhesion and proliferation, and it deserves more in-depth study in the future research.

In order to evaluate the new bone formation, the femoral condyle bone defect model of the rabbits was created and the nanofibrous scaffolds were implanted in the defect site. The Micro-CT and histology results showed that PCL/dB-ECM (2:1) nanofibrous scaffold could induce more bone regeneration compared with the other scaffolds. Even more remarkably, the new formation bone tissue exhibited good trabecular microstructure, as well as great integration with the surrounding native bone tissue. In contrast, the PCL nanofibrous scaffold showed extremely insufficient new bone formation. It can be found from the gross observation that PCL nanofibrous scaffold hardly degraded after 12 weeks of implantation in vivo, indicating that it may inhibit new bone formation. Even though PCL is biodegradable, it still takes a long time to completely degrade[58, 59], which is not suitable for the construction of BTE scaffolds. It was expected that the rate of degradation of biomaterials which were used in the field of BTE should be similar to the rate of bone regeneration. Too slow degradation rate led to residual scaffold at the defect site, thus hindering the new bone formation[60, 61]. Considering this, the incorporation of dB-ECM into the nanofibrous scaffolds not only improved the bioactivity of PCL, but also accelerated the degradation of scaffolds, making them more inclined to promote new bone formation.

5. Conclusion

In this study, dB-ECM was prepared successfully by decellularizing process, and subsequently, the PCL/dB-ECM nanofibrous scaffolds were fabricated using electrospinning. The microstructure of the PCL/dB-ECM nanofibrous scaffolds exhibited randomly arranged nanofibers interlaced to each other to form a network structure. The incorporation of dB-ECM into the scaffolds improved the bioactivity of PCL and significantly enhanced the attachment, proliferation and osteogenic differentiation of rBMSCs. Furthermore, in vivo experiment demonstrated that PCL/dB-ECM (2:1) nanofibrous scaffold remarkably promoted new bone formation. Hence, this work advanced our knowledge about construction of dB-ECM-based nanostructure scaffolds and provided a promising strategy for bone defect treatment.

Abbreviations

Abbreviations

PCL poly(ε-caprolactone)

dB-ECM decellularized bone extracellular matrix

rBMSCs rabbit bone mesenchymal stem cells

BTE bone tissue engineering

3D three dimension

PLA poly(lactic acid)

PLGA poly(lactic-co-glycolic acid)

Micro-CT micro-computed tomography

SEM scanning electron microscope

EDS energy-dispersive spectrometer

WAR water contact angle

CLSM confocal laser scanning microscope

ALP alkaline phosphatase

ARS Alizarin Red S

Declarations

Ethics approval and consent to participate

The animal study was carried out in compliance with the regulations and guidelines of the Ethics Commission of Nanjing Medical University.

Consent for publication

All authors agreed to publish.

Availability of data and materials

The datasets used and/or analysed during the current study are available from

the corresponding author on reasonable request.

Competing interests

The authors declare that they have no competing interests.

Funding

This work was supported by Municipal Science and Technology Bureau of Jiangning district, Nanjing, China (20212021NJNQKJHMJHXM0133).

Author's contributions

M.Z and L.L designed the study. M.Z, Q.Z and Q.D performed the experiments. J.Z, X.Z and H.H collected the data. J.B, H.S and F.S analyzed the data. M.Z and Q.Z wrote the manuscript. L.L revised the manuscript and supervised the findings of this study. All authors read and approved the final manuscript.

Acknowledgements

None

References

1. Wauthle R, van der Stok J, Yavari SA, Humbeeck JV, Kruth JP, Zadpoor AA, Weinans H, Mulier M, Schrooten J. Additively manufactured porous tantalum implants. Acta Biomater. 2015;14:217–25.
2. Schemitsch EH. Size Matters: Defining Critical in Bone Defect Size. J Orthop Trauma. 2017;31(Suppl 5):20–2.
3. Campana V, Milano G, Pagano E, Barba M, Cicione C, Salonna G, Lattanzi W, Logroscino G. Bone substitutes in orthopaedic surgery: from basic science to clinical practice. J Mater Sci Mater Med. 2014;25(10):2445–61.
4. Lee DJ, Diachina S, Lee YT, Zhao L, Zou R, Tang N, Han H, Chen X, Ko CC. Decellularized bone matrix grafts for calvaria regeneration. J Tissue Eng. 2016;7:2041731416680306.

5. Roddy E, DeBaun MR, Daoud-Gray A, Yang YP, Gardner MJ. Treatment of critical-sized bone defects: clinical and tissue engineering perspectives. Eur J Orthop Surg Traumatol. 2018;28(3):351–62.
6. Rindone AN, Nyberg E, Grayson WL. 3D-Printing Composite Polycaprolactone-Decellularized Bone Matrix Scaffolds for Bone Tissue Engineering Applications. Methods Mol Biol. 2018;1577:209–26.
7. Chen G, Dong C, Yang L, Lv Y. 3D Scaffolds with Different Stiffness but the Same Microstructure for Bone Tissue Engineering. ACS Appl Mater Interfaces. 2015;7(29):15790–802.
8. Carvalho MS, Silva JC, Udangawa RN, Cabral JMS, Ferreira FC, da Silva CL, Linhardt RJ, Vashishth D. Co-culture cell-derived extracellular matrix loaded electrospun microfibrous scaffolds for bone tissue engineering. Mater Sci Eng C Mater Biol Appl. 2019;99:479–90.
9. Tebyanian H, Norahan MH, Eyni H, Movahedin M, Mortazavi SJ, Karami A, Nourani MR, Baheiraei N. Effects of collagen/β-tricalcium phosphate bone graft to regenerate bone in critically sized rabbit calvarial defects. J Appl Biomater Funct Mater. 2019;17(1):2280800018820490.
10. Musumeci G, Castrogiovanni P, Leonardi R, Trovato FM, Szychlinska MA, Giunta AD, Loreto C, Castorina S. New perspectives for articular cartilage repair treatment through tissue engineering: A contemporary review. World J Orthop. 2014;5(2):80–8.
11. Hong J, Yeo M, Yang GH, Kim G. Cell-Electrospinning and Its Application for Tissue Engineering. Int J Mol Sci. 2019. 20(24).
12. Li Y, Tian J, Yang C, Hsiao BS. Nanocomposite Film Containing Fibrous Cellulose Scaffold and Ag/TiO_2 Nanoparticles and Its Antibacterial Activity. Polymers (Basel). 2018. 10(10).
13. Patel KD, Kim TH, Mandakhbayar N, Singh RK, Jang JH, Lee JH, Kim HW. Coating biopolymer nanofibers with carbon nanotubes accelerates tissue healing and bone regeneration through orchestrated cell- and tissue-regulatory responses. Acta Biomater. 2020;108:97–110.
14. Bharadwaz A, Jayasuriya AC. Recent trends in the application of widely used natural and synthetic polymer nanocomposites in bone tissue regeneration. Mater Sci Eng C Mater Biol Appl. 2020;110:110698.
15. Elgali I, Omar O, Dahlin C, Thomsen P. Guided bone regeneration: materials and biological mechanisms revisited. Eur J Oral Sci. 2017;125(5):315–37.
16. Park JY, Shim JH, Choi SA, Jang J, Kim MK, Lee SH. D.W. Cho, 3D printing technology to control BMP-2 and VEGF delivery spatially and temporally to promote large-volume bone regeneration. J Mater Chem B. 2015;3(27):5415–25.
17. Dikici BA, Dikici S, Reilly GC, MacNeil S, Claeyssens F. A Novel Bilayer Polycaprolactone Membrane for Guided Bone Regeneration: Combining Electrospinning and Emulsion Templating. Materials (Basel). 2019. 12(16).
18. Wang J, Wang L, Zhou Z, Lai H, Xu P, Liao L, Wei J. Biodegradable Polymer Membranes Applied in Guided Bone/Tissue Regeneration: A Review. Polymers (Basel). 2016. 8(4).
19. Trachtenberg JE, Santoro M, C3rd. Williams, Piard CM, Smith BT, Placone JK, Menegaz BA, Molina ER, Lamhamedi-Cherradi SE, Ludwig JA, Sikavitsas VI, Fisher JP, Mikos AG. Effects of Shear Stress

Gradients on Ewing Sarcoma Cells Using 3D Printed Scaffolds and Flow Perfusion. ACS Biomater Sci Eng. 2018;4(2):347–56.

20. Miroshnichenko S, Timofeeva V, Permykova E, Ershov S, Kiryukhantsev-Korneer P, Dvořaková E, Shtansky D, Zajíčková L, Solovieva A, Manakhov A. Plasma-Coated Polycaprolactone Nanofibers with Covalently Bonded Platelet-Rich Plasma Enhance Adhesion and Growth of Human Fibroblasts. Nanomaterials (Basel). 2019. 9(4).
21. Richbourg NR, Peppas NA, Sikavitsas VI. Tuning the biomimetic behavior of scaffolds for regenerative medicine through surface modifications. J Tissue Eng Regen Med. 2019;13(8):1275–93.
22. Ren K, Wang Y, Sun T, Yue W, Zhang H. Electrospun PCL/gelatin composite nanofiber structures for effective guided bone regeneration membranes. Mater Sci Eng C Mater Biol Appl. 2017;78:324–32.
23. Hu S, Chen H, Zhou X, Chen G, Hu K, Cheng Y, Wang L, Zhang F. Thermally induced self-agglomeration 3D scaffolds with BMP-2-loaded core-shell fibers for enhanced osteogenic differentiation of rat adipose-derived stem cells. Int J Nanomedicine. 2018;13:4145–55.
24. Jorgensen AM, Chou Z, Gillispie G, Lee SJ, Yoo JJ, Soker S, Atala A. Decellularized Skin Extracellular Matrix (dsECM) Improves the Physical and Biological Properties of Fibrinogen Hydrogel for Skin Bioprinting Applications. Nanomaterials (Basel). 2020. 10(8).
25. Mohiuddin OA, Campbell B, Poche JN, Michelle M, Rogers E, Gaupp D, Harrison MAA, Bunnel BA, Hayes DJ, Gimble JM. Decellularized Adipose Tissue Hydrogel Promotes Bone Regeneration in Critical-Sized Mouse Femoral Defect Model. Front Bioeng Biotechnol. 2019;7:211.
26. Taylor B, Indano S, Yankannah Y, Patel P, Perez XI, Freeman J. Decellularized Cortical Bone Scaffold Promotes Organized Neovascularization In Vivo. Tissue Eng Part A. 2019;25(13–14):964–77.
27. Parmaksiz M, Elçin AE, Elçin YM. Decellularized bovine small intestinal submucosa-PCL/hydroxyapatite-based multilayer composite scaffold for hard tissue repair. Mater Sci Eng C Mater Biol Appl. 2019;94:788–97.
28. Benders KE, van Weeren PR, Badylak SF, Saris DB, Dhert WJ, Malda J. Extracellular matrix scaffolds for cartilage and bone regeneration. Trends Biotechnol. 2013;31(3):169–76.
29. Kim YS, Majid M, Melchiorri AJ, Mikos AG. Applications of decellularized extracellular matrix in bone and cartilage tissue engineering. Bioeng Transl Med. 2019;4(1):83–95.
30. Chen G, Lv Y. Decellularized Bone Matrix Scaffold for Bone Regeneration. Methods Mol Biol. 2018;1577:239–54.
31. Kim JY, Ahn G, Kim C, Lee JS, Lee IG, An SH, Yun WS, Kim SY, Shim JH. Synergistic Effects of Beta Tri-Calcium Phosphate and Porcine-Derived Decellularized Bone Extracellular Matrix in 3D-Printed Polycaprolactone Scaffold on Bone Regeneration. Macromol Biosci. 2018;18(6):e1800025.
32. Crapo PM, Gilbert TW, Badylak SF. An overview of tissue and whole organ decellularization processes. Biomaterials. 2011;32(12):3233–43.
33. Chen K, Lin X, Zhang Q, Ni J, Li J, Xiao J, Wang Y, Ye Y, Chen L, Jin K, Chen L. Decellularized periosteum as a potential biologic scaffold for bone tissue engineering. Acta Biomater. 2015;19:46–

55.

34. Wu J, Ding Q, Dutta A, Wang Y, Huang YH, Weng H, Tang L, Hong Y. An injectable extracellular matrix derived hydrogel for meniscus repair and regeneration. Acta Biomater. 2015;16:49–59.
35. Dong Q, Zhang M, Zhou X, Shao Y, Li J, Wang L, Chu C, Xue F, Yao Q. J. Bai, 3D-printed Mg-incorporated PCL-based scaffolds: A promising approach for bone healing. Mater Sci Eng C Mater Biol Appl. 2021;129:112372.
36. Wang Z, Lin M, Xie Q, Sun H, Huang Y, Zhang D, Yu Z, Bi X, Chen J, Wang J, Shi W, Gu P, Fan X. Electrospun silk fibroin/poly(lactide-co-ε-caprolactone) nanofibrous scaffolds for bone regeneration. Int J Nanomedicine. 2016;11:1483–500.
37. Yazdanpanah Z, Johnston JD, Cooper D, Chen X. 3D Bioprinted Scaffolds for Bone Tissue Engineering: State-Of-The-Art and Emerging Technologies. Front Bioeng Biotechnol. 2022;10:824156.
38. Wang Z, Wang Y, Yan J, Zhang K, Lin F, Xiang L, Deng L, Guan Z, Cui W, Zhang H. Pharmaceutical electrospinning and 3D printing scaffold design for bone regeneration. Adv Drug Deliv Rev. 2021;174:504–34.
39. Fairag R, Li L, Ramirez-GarciaLuna JL, Taylor MS, Gaerke B, Weber MH, Rosenzweig DH, Haglund L. A Composite Lactide-Mineral 3D-Printed Scaffold for Bone Repair and Regeneration. Front Cell Dev Biol. 2021;9:654518.
40. Hao Z, Song Z, Huang J, Huang K, Panetta A, Gu Z, Wu J. The scaffold microenvironment for stem cell based bone tissue engineering. Biomater Sci. 2017;5(8):1382–92.
41. Perez RA, Mestres G. Role of pore size and morphology in musculo-skeletal tissue regeneration. Mater Sci Eng C Mater Biol Appl. 2016;61:922–39.
42. Söhling N, Neijhoft J, Nienhaus V, Acker V, Harbig J, Menz F, Ochs J, Verboket RD, Ritz U, Blaeser A, Dörsam E, Frank J, Marzi I. D. Henrich, 3D-Printing of Hierarchically Designed and Osteoconductive Bone Tissue Engineering Scaffolds. Materials (Basel). 2020. 13(8).
43. Keshvardoostchokami M, Majidi SS, Huo P, Ramachandran R, Chen M, Liu B, Electrospun Nanofibers of Natural and Synthetic Polymers as Artificial Extracellular Matrix for Tissue Engineering. Nanomaterials (Basel). 2020. 11(1).
44. Chahal S, Kumar A, Hussian F. Development of biomimetic electrospun polymeric biomaterials for bone tissue engineering. A review. J Biomater Sci Polym Ed. 2019;30(14):1308–55.
45. Horner CB, Maldonado M, Tai Y, Rony R, Nam J. Spatially Regulated Multiphenotypic Differentiation of Stem Cells in 3D via Engineered Mechanical Gradient. ACS Appl Mater Interfaces. 2019;11(49):45479–88.
46. Damaraju SM, Shen Y, Elele E, Khusid B, Eshghinejad A, Li J, Jaffe M, Arinzeh TL. Three-dimensional piezoelectric fibrous scaffolds selectively promote mesenchymal stem cell differentiation. Biomaterials. 2017;149:51–62.
47. Yuan B, Wang Z, Zhao Y, Tang Y, Zhou S, Sun Y, Chen X. In Vitro and In Vivo Study of a Novel Nanoscale Demineralized Bone Matrix Coated PCL/β-TCP Scaffold for Bone Regeneration. Macromol Biosci. 2021;21(3):e2000336.

48. Wubneh A, Tsekoura EK, Ayranci C, Uludağ H. Current state of fabrication technologies and materials for bone tissue engineering. Acta Biomater. 2018;80:1–30.
49. Bahraminasab M, Janmohammadi M, Arab S, Talebi A, Nooshabadi VT, Koohsarian P, Nourbakhsh MS. Bone Scaffolds: An Incorporation of Biomaterials, Cells, and Biofactors. ACS Biomater Sci Eng. 2021;7(12):5397–431.
50. Oh GW, Nguyen VT, Heo SY, Ko SC, Kim CS, Park WS, Choi IW. W.K. Jung, 3D PCL/fish collagen composite scaffolds incorporating osteogenic abalone protein hydrolysates for bone regeneration application: in vitro and in vivo studies. J Biomater Sci Polym Ed. 2021;32(3):355–71.
51. Perić K, Rider P, Alkildani S, Retnasingh S, Pejakić M, Schnettler R, Gosau M, Smeets R, Jung O, Barbeck M. An introduction to bone tissue engineering. Int J Artif Organs. 2020;43(2):69–86.
52. Seddighian A, Ganji F, Baghaban-Eslaminejad M, Bagheri F. Electrospun PCL scaffold modified with chitosan nanoparticles for enhanced bone regeneration. Prog Biomater. 2021;10(1):65–76.
53. Dong C, Qiao F, Chen G, Lv Y. Demineralized and decellularized bone extracellular matrix-incorporated electrospun nanofibrous scaffold for bone regeneration. J Mater Chem B. 2021;9(34):6881–94.
54. Frantz C, Stewart KM, Weaver VM. The extracellular matrix at a glance. J Cell Sci. 2010;123(Pt 24):4195–200.
55. Taylor DA, Sampaio LC, Ferdous Z, Gobin AS, Taite LJ. Decellularized matrices in regenerative medicine. Acta Biomater. 2018;74:74–89.
56. Kabirian F, Mozafari M. Decellularized ECM-derived bioinks: Prospects for the future. Methods. 2020;171:108–18.
57. Smith CA, Board TN, Rooney P, Eagle MJ, Richardson SM, Hoyland JA. Human decellularized bone scaffolds from aged donors show improved osteoinductive capacity compared to young donor bone. PLoS ONE. 2017;12(5):e0177416.
58. Gleadall A, Pan J, Kruft MA, Kellomäki M. Degradation mechanisms of bioresorbable polyesters. Part 1. Effects of random scission, end scission and autocatalysis. Acta Biomater. 2014;10(5):2223–32.
59. Gleadall A, Pan J, Kruft MA, Kellomäki M. Degradation mechanisms of bioresorbable polyesters. Part 2. Effects of initial molecular weight and residual monomer. Acta Biomater. 2014;10(5):2233–40.
60. Yildirimer L, Seifalian AM. Three-dimensional biomaterial degradation - Material choice, design and extrinsic factor considerations. Biotechnol Adv. 2014;32(5):984–99.
61. Malikmammadov E, Tanir TE, Kiziltay A, Hasirci V, Hasirci N. PCL and PCL-based materials in biomedical applications. J Biomater Sci Polym Ed. 2018;29(7–9):863–93.

Figures

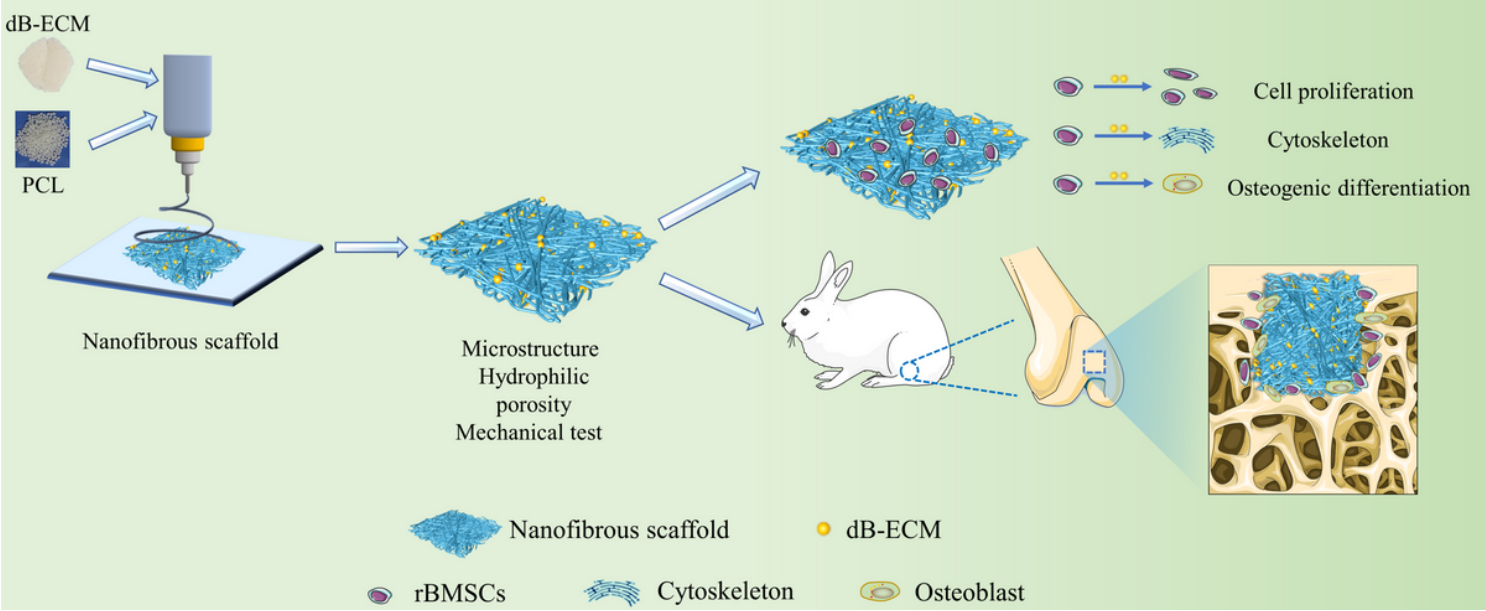

Figure 1

Schematic of fabrication of PCL/dB-ECM nanofibrous scaffolds and subsequent in vitro and in vivo studies.

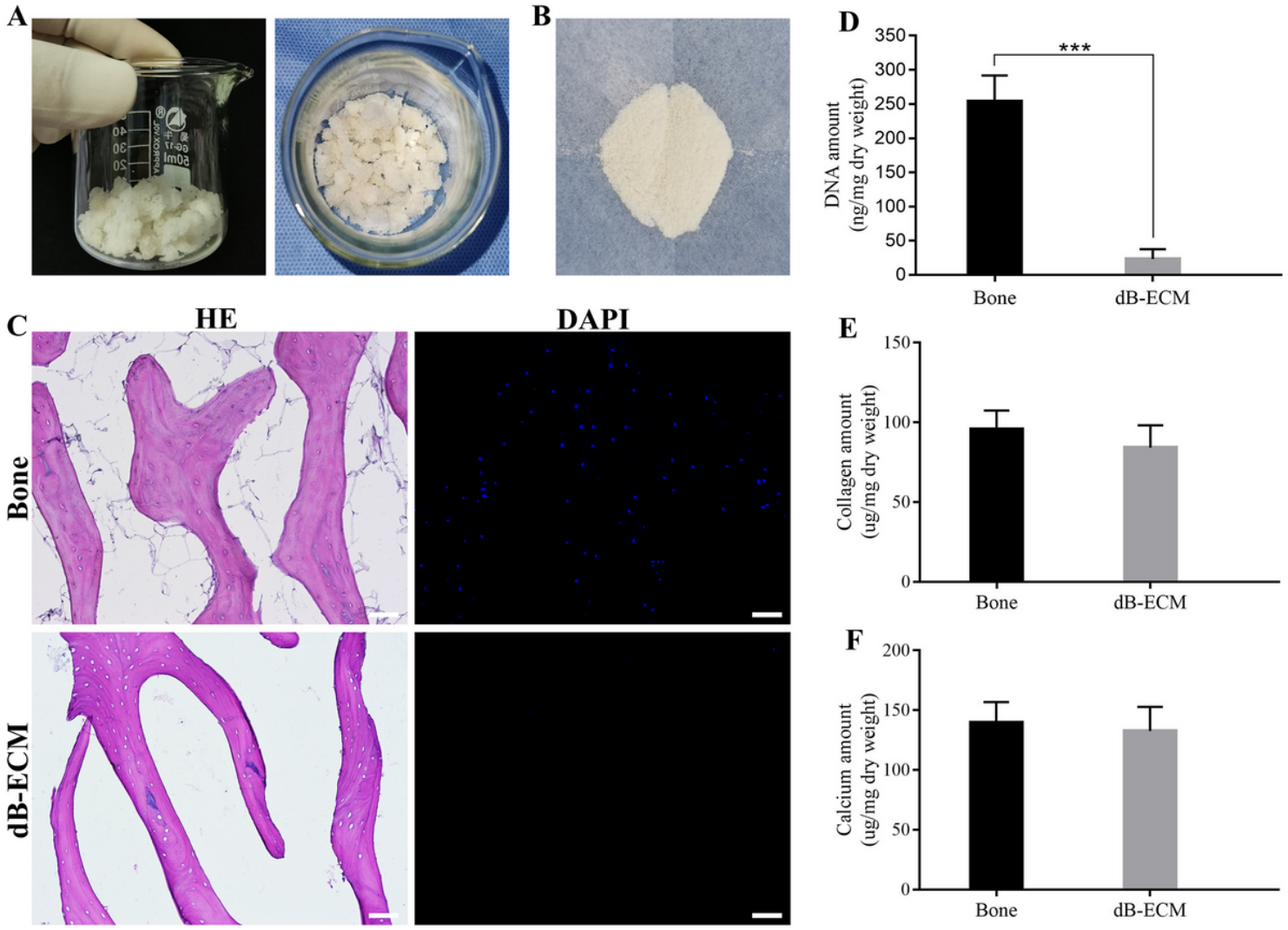

Figure 2

Preparation and characterization of dB-ECM. (A) Gross observation of the dB-ECM. (B) dB-ECM powders used in this study. (C-D) Evaluation of decellularization effect of dB-ECM by H&E, DAPI staining and DNA quantification. Scale bar = 100 μm. (E-F) Quantitative analysis of the collagen and calcium in native bone and dB-ECM. (***, $p < 0.001$).

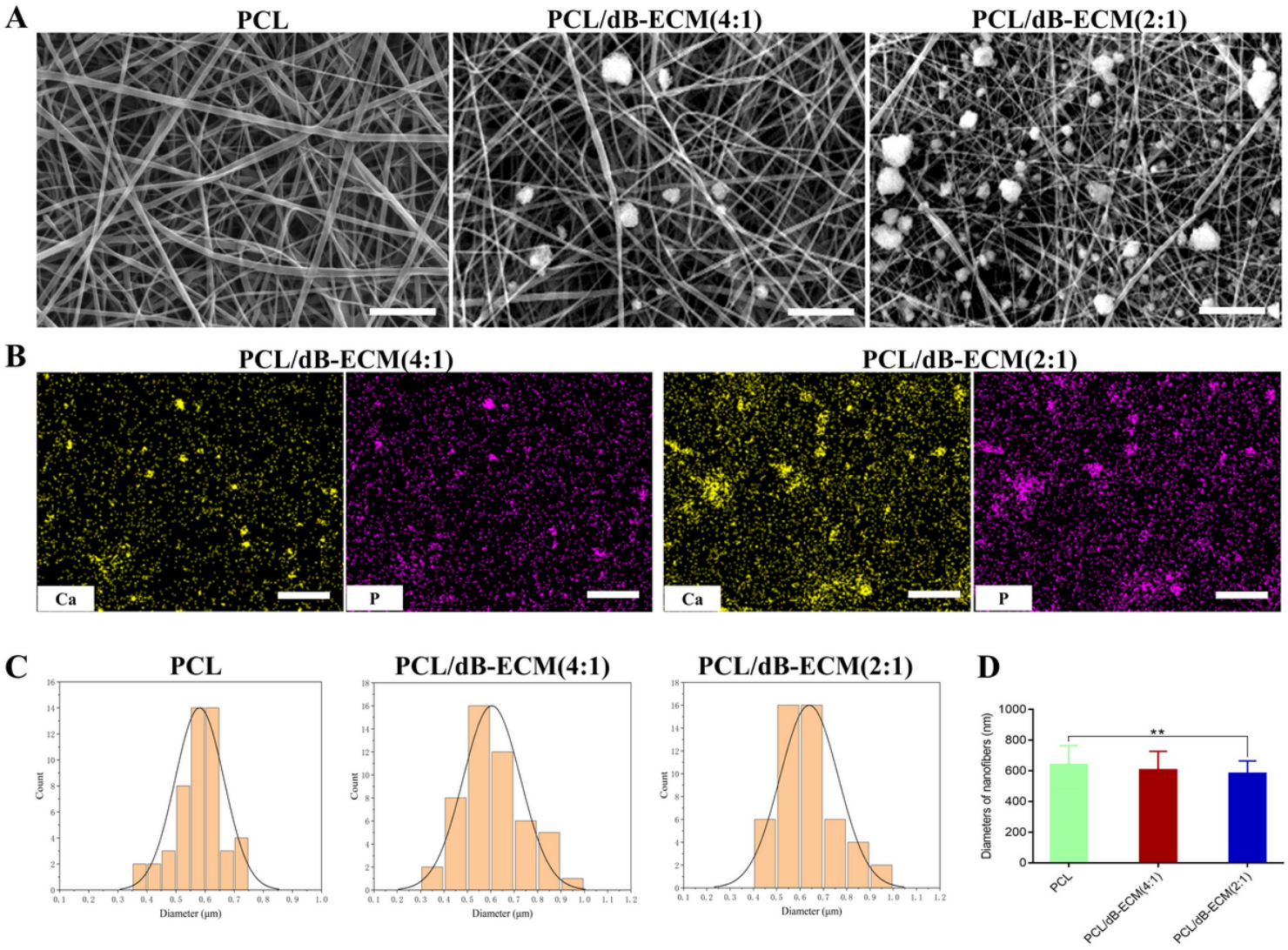

Figure 3

The microstructure of the nanofibrous scaffolds. (A) SEM images of the nanofibrous scaffolds. Scale bar = 10 μm. (B) EDS mapping distribution of Ca and P elements in PCL/dB-ECM (4:1) and PCL/dB-ECM (2:1) nanofibrous scaffolds. Scale bar = 25 μm. (C-D) The diameter distribution and average diameter of nanofibers in the three groups of scaffolds measured from SEM images with Image J. (**, $p < 0.01$).

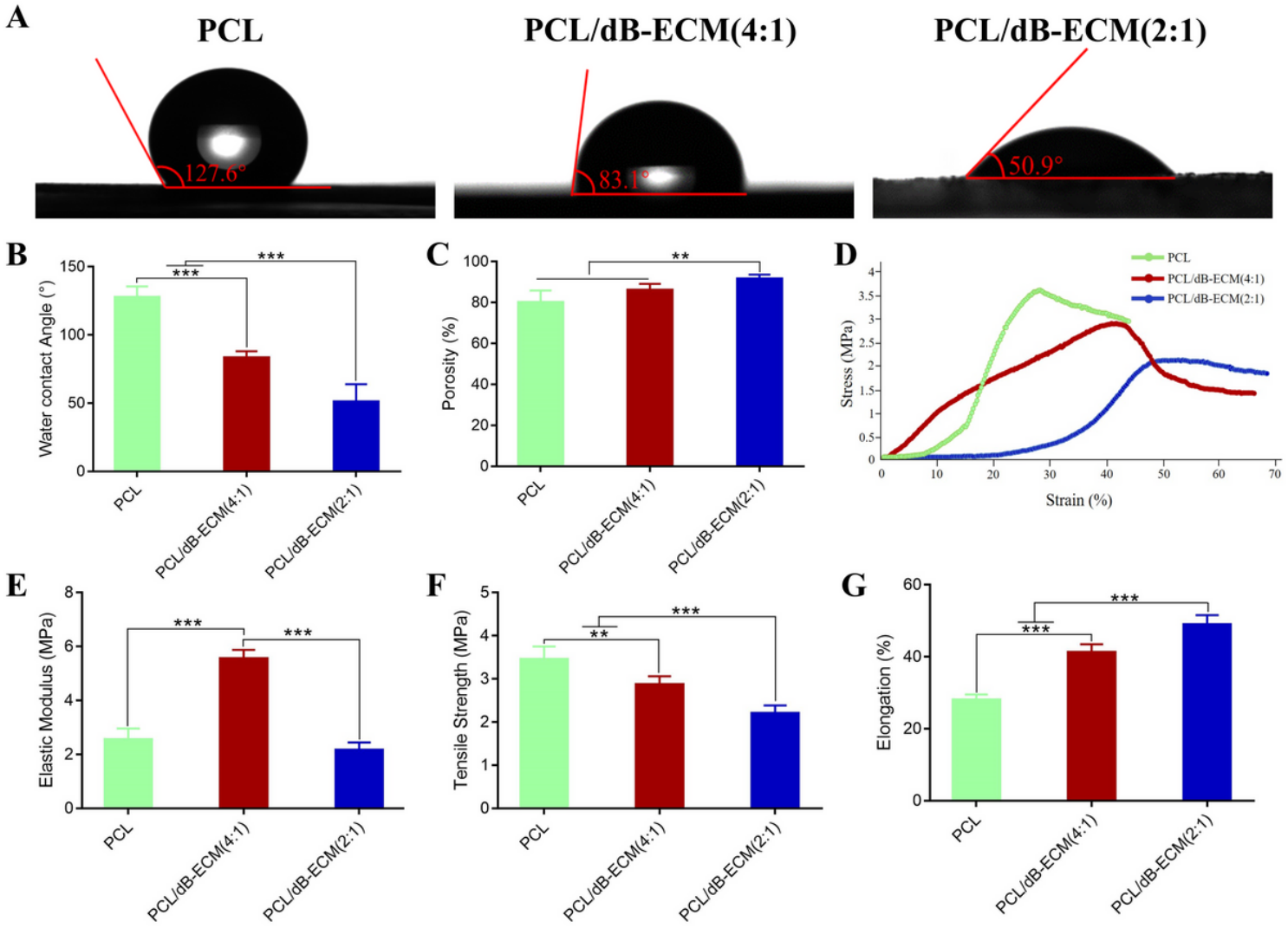

Figure 4

Hydrophilicity, porosity analysis and mechanical test of the nanofibrous scaffolds. (A-B) Water contact angle analysis showing the hydrophilicity of the nanofibrous scaffolds. (C) Porosity analysis of the nanofibrous scaffolds. (D) Stress-strain curve showing the tensile mechanical properties of the nanofibrous scaffolds. (E) Elastic modulus of the nanofibrous scaffolds. (F) Tensile strength showing the highest stress prior to the nanofibrous scaffolds break. (G) Elongation (%) showing the percentage elongation of the nanofibrous scaffolds at the break. (**, $p < 0.01$; ***, $p < 0.001$).

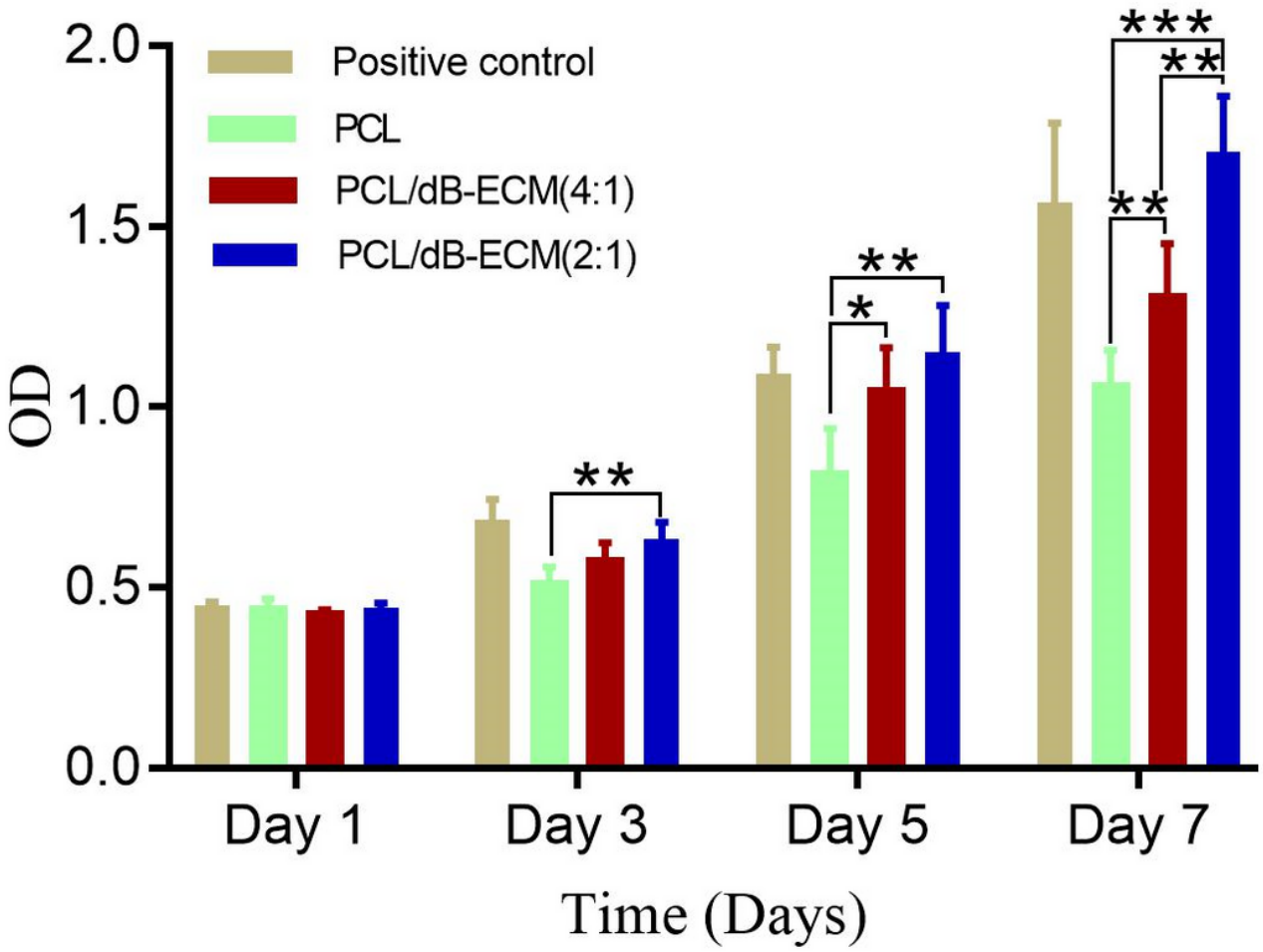

Figure 5

The CCK-8 test results showing the cell proliferation of rBMSCs cultured on nanofibrous scaffolds at 1, 3, 5 and 7 days. (*, $p < 0.05$; **, $p < 0.01$; ***, $p < 0.001$).

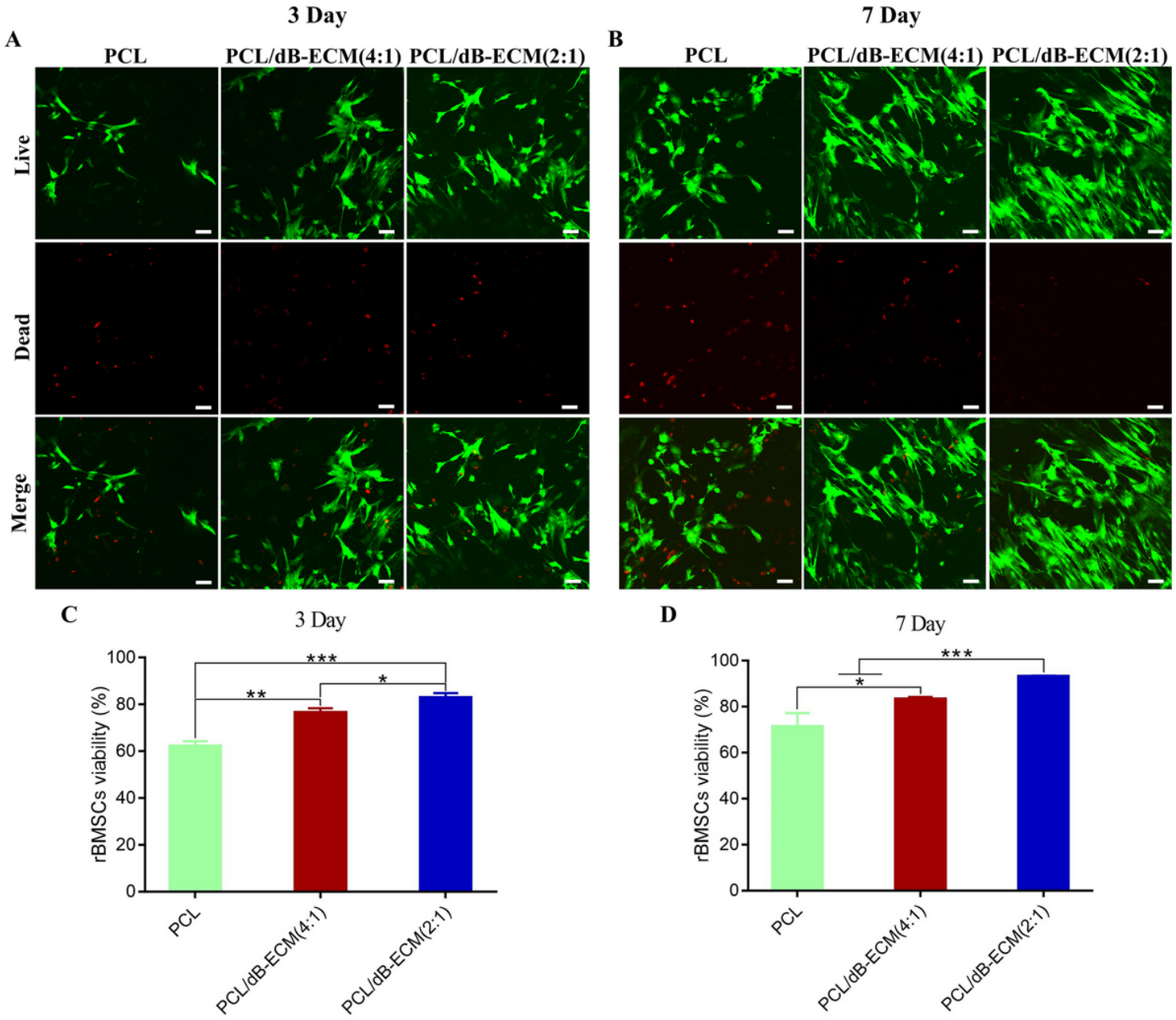

Figure 6

Cell viability of the nanofibrous scaffolds assessed by Live-Dead staining. (A) Representative images of Live-Dead staining showing viability of rBMSCs cultured on nanofibrous scaffolds for 3 days. Scale bar = 50 μm. (B) Representative images of Live-Dead staining showing viability of rBMSCs cultured on nanofibrous scaffolds for 7 days. Scale bar = 50 μm. (C-D) Quantification of rBMSCs viability calculated from Live-Dead images with Image J after 3 and 7 days cultured on nanofibrous scaffolds, respectively. (*, $p < 0.05$; **, $p < 0.01$; ***, $p < 0.001$).

3.3.3 Cell morphology observation

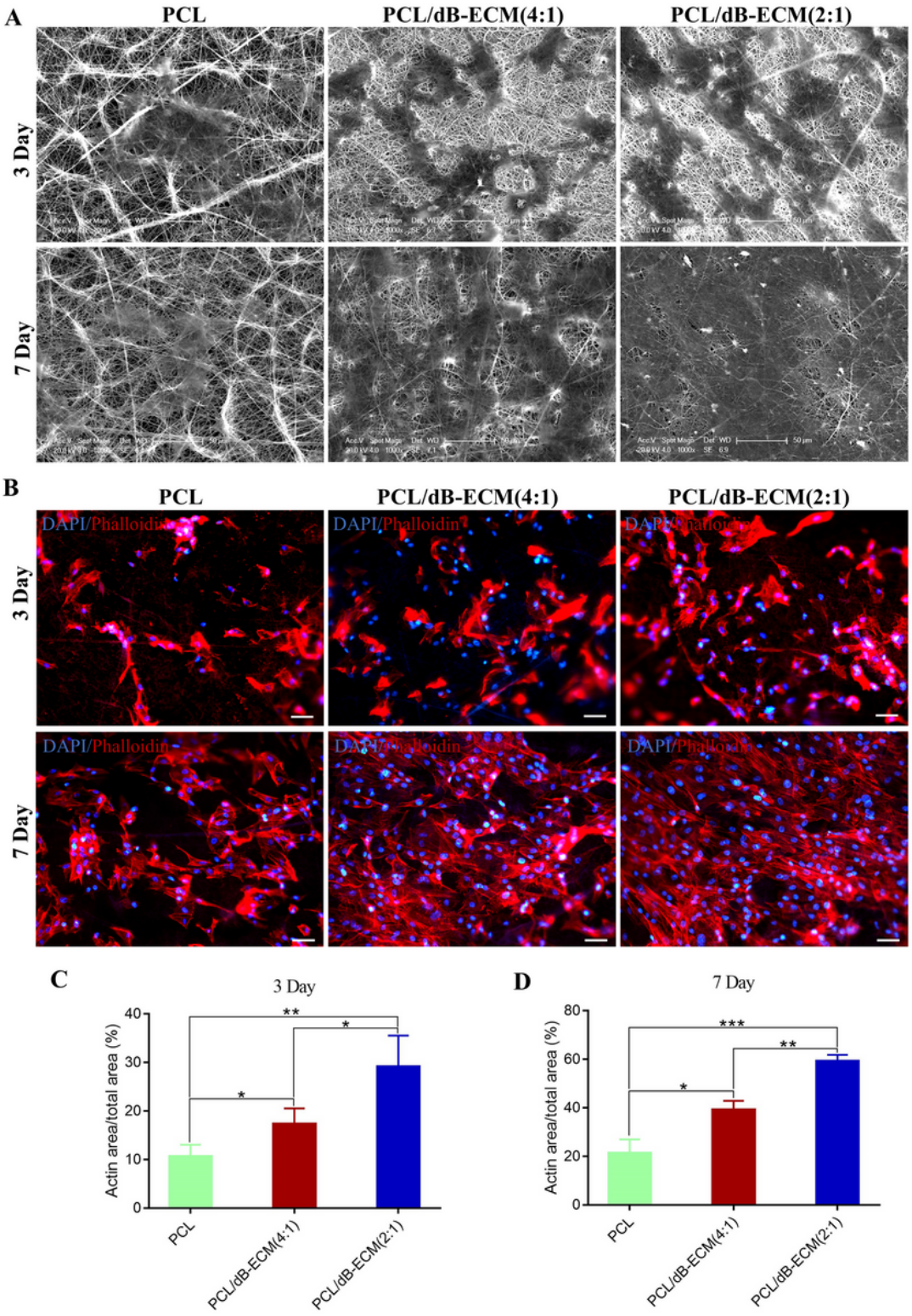

Figure 7

Evaluation of morphology and cytoskeleton extension of rBMSCs cultured on nanofibrous scaffolds. (A) Representative images of SEM showing morphology of rBMSCs cultured on nanofibrous scaffolds for 3 and 7 days. Scale bar = 50 μm. (B) Representative images of F-actin staining showing cytoskeleton spread and extension of rBMSCs cultured on nanofibrous scaffolds for 3 and 7 days. Scale bar = 50 μm.

(C-D) Quantitative analysis of actin area of rBMSCs cultured on nanofibrous scaffolds on day 3 and day 7 calculated from F-actin staining images with Image J. (*, p < 0.05; **, p < 0.01; ***, p < 0.001).

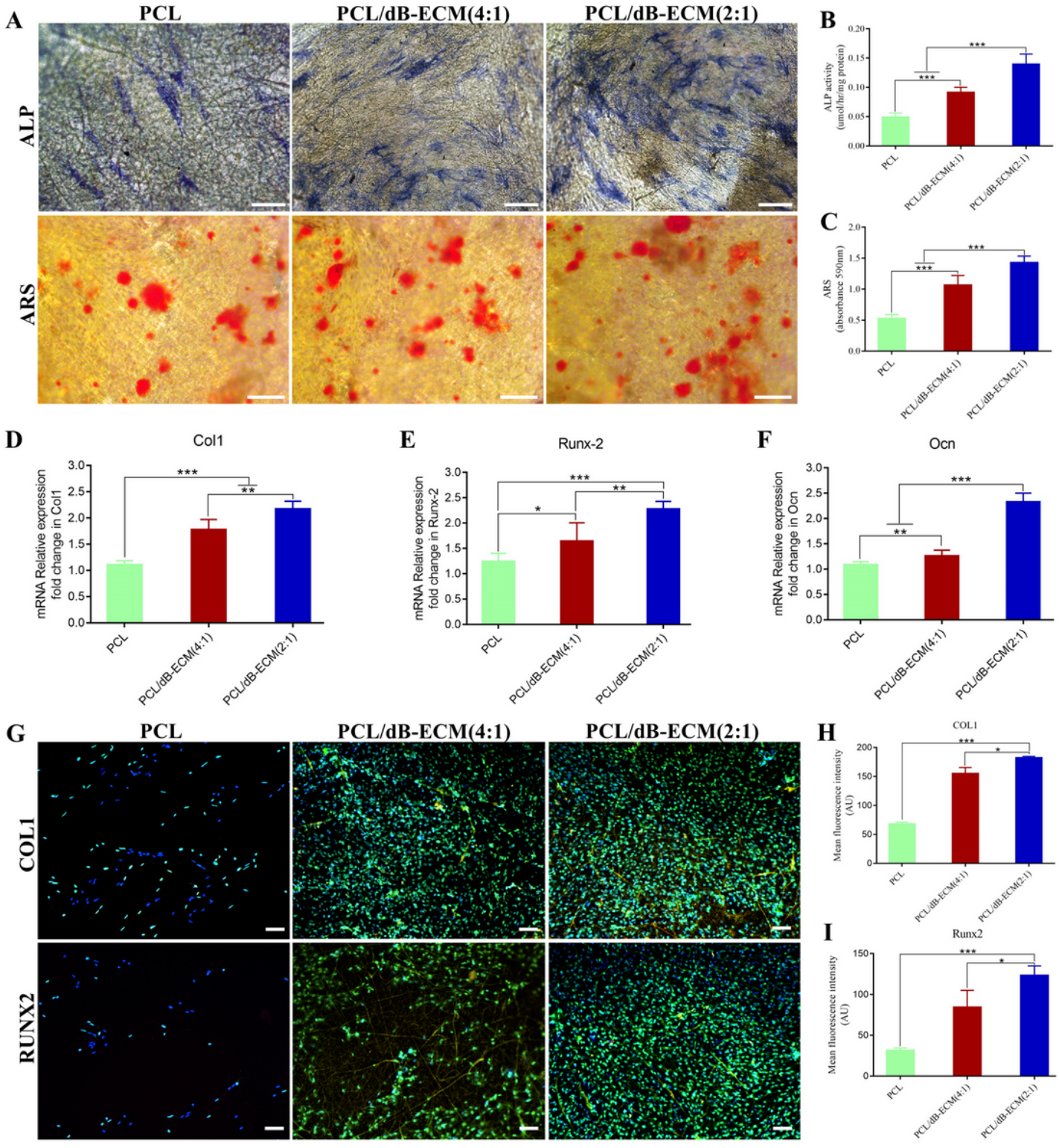

Figure 8

PCL/dB-ECM (2:1) nanofibrous scaffold promoted osteogenic differentiation of rBMSCs in vitro. (A) Representative microscopic images showing ALP activity and calcium deposition by ALP staining and

ARS staining, respectively. Scale bar = 100 μm. (B) Quantification of ALP activity of rBMSCs cultured on nanofibrous scaffolds on day 7. (C) Quantitative analysis of ARS staining of rBMSCs cultured on nanofibrous scaffolds on day 21. Osteogenic-related genes expression Col1 (D), Runx2 (E), and Ocn (F) analyzed by qRT-PCR. (G) Representative immunofluorescent images showing expression of osteogenic-related proteins by rBMSCs cultured on nanofibrous scaffolds for 14 days. Scale bar = 100 μm. Quantitative analysis of the fluorescence intensity of osteogenic-related proteins Col1 (H) and Runx2 (I) analyzed from immunofluorescent images with Image J. (*, $p < 0.05$; **, $p < 0.01$; ***, $p < 0.001$).

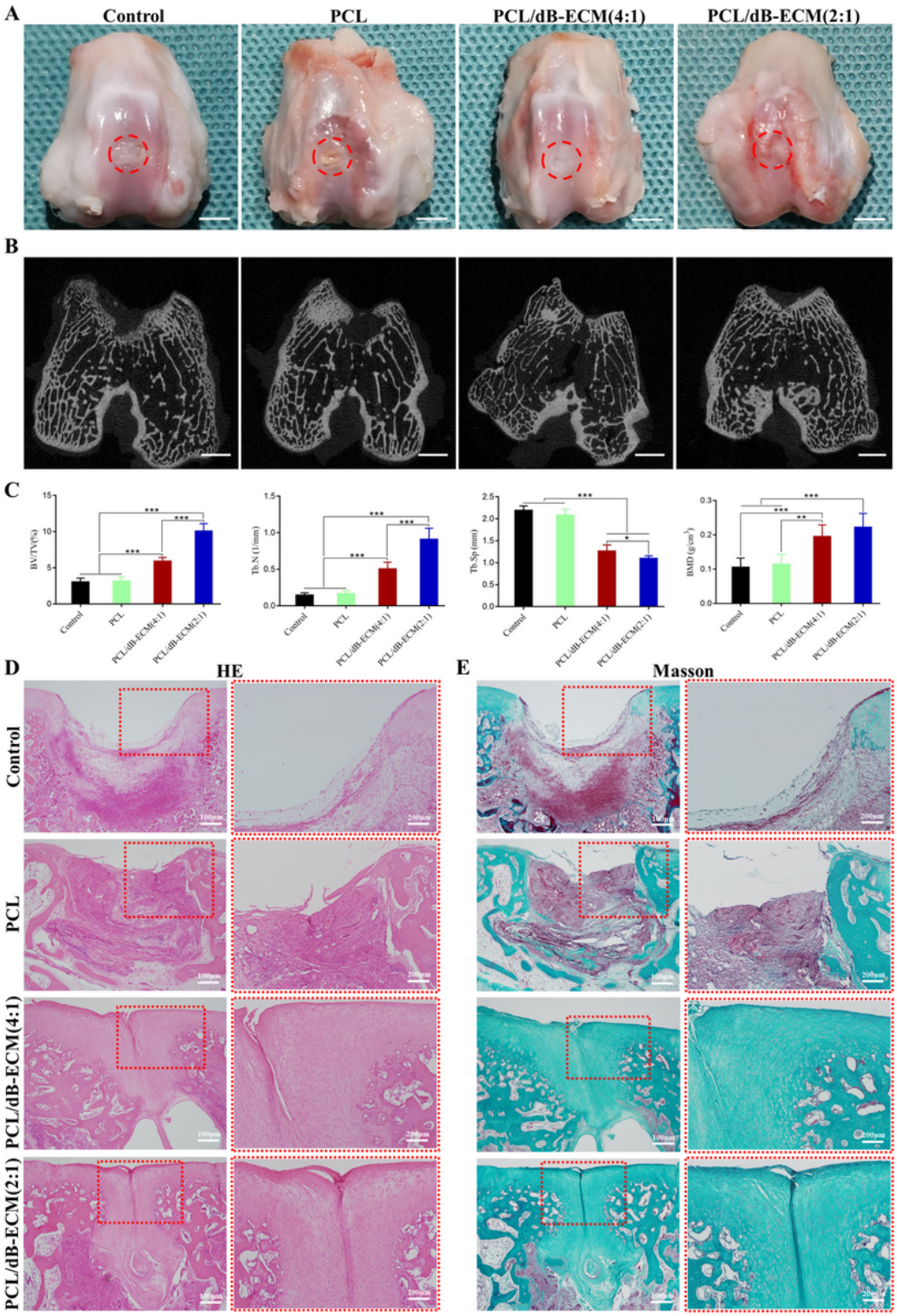

Figure 9

PCL/dB-ECM (2:1) nanofibrous scaffold promoted osteogenesis in vivo. (A) Gross observation of rabbit femoral condyle bone defect model repaired with no implant, PCL, PCL/dB-ECM (4:1) and PCL/dB-ECM (2:1) nanofibrous scaffolds. Scale bar = 5 mm. (B) Representative Micro-CT images showing the new bone formation and microstructure of the regenerated trabecular within the defect area. Scale bar = 5 mm. (C) Quantitative analysis of mineralized callus volume fraction (BV/TV), trabecular number (Tb. N), trabecular separation (Tb. Sp) (BV/TV, %) and bone mineral density (BMD, g/cm^3). (D) H&E staining images of regenerated bone tissue at 12 weeks after surgery. (E) Masson trichrome staining images of regenerated bone tissue at 12 weeks after surgery. (*, $p < 0.05$; **, $p < 0.01$; ***, $p < 0.001$).